COARSE-GRAINED MOLECULAR DYNAMICS SIMULATION APPROACH TO HIGH-DENSITY LIPOPROTEIN-MIMETICS MODELING

A Dissertation
Presented to
The Academic Faculty

by

Taeyoung Kim

In Partial Fulfillment
of the Requirements for the Degree
Doctor of Philosophy in the
George W. Woodruff School of Mechanical Engineering

Georgia Institute of Technology
December 2019

COARSE-GRAINED MOLECULAR DYNAMICS SIMULATION APPROACH TO HIGH-DENSITY LIPOPROTEIN-MIMETICS MODELING

Approved by:

Dr. YongTae Kim, Advisor
School of Mechanical Engineering
Georgia Institute of Technology

Dr. Seung Soon Jang
School of Materials Science and Engineering
Georgia Institute of Technology

Dr. David Ku
School of Mechanical Engineering
Georgia Institute of Technology

Dr. Ravi Kane
School of Chemical & Biomolecular Engineering
Georgia Institute of Technology

Dr. Todd Sulchek
School of Mechanical Engineering
Georgia Institute of Technology

Date Approved: [08/15/2019]

ACKNOWLEDGEMENTS

My 3-year PhD life was so intense with qualifying exam, proposal and defense. I could have never achieved my PhD degree without thankful people surrounding me for just 3 years, comparing others who do normally 4-5 years. I would like to thank to people who helped me a lot in this acknowledgements section.

To my love Heejin Kim. You followed me here outside of our home country, giving up many things. I would thank for your belief on me. Obviously, you helped me a lot in many ways. You always encouraged me, and you were always on my side. I could not have achieved PhD degree without you. Thank you and I love you.

To my family. Hyoung suk Kim, Young ja Kwon, Han lim Kim, and Hyangyoung Park. I am sure that you were worried about me when I decided to go abroad to study at a late age. However, you always believed and supported me. Your presence always means a lot to me. Thank you.

To my friends. You are like oasis in desert. Although my PhD life was so dry and stressful, I could manage my stress level with you. My lab mates, especially, Dr. Yoshitaka Sei and Dr. Jinhwan “Jaden” Kim, helped me who was novice in experiments in bioscience. Besides, you always gave me valuable comments regarding proposal, defense, and conference presentation preparations. In addition, I thank to Dr. Sang Eun Jee, who introduced me a new field, Molecular Dynamics (MD) simulation. You are the best teacher I have ever met in my life. Although I was familiar with computation, I could not have learned this field of study so fast without you. While my family members provided

psychological stability, you gave me practical help. Thank you. It was impossible to graduate so fast without you.

To my advisor Dr. YongTae “Tony” Kim. I thank you for giving me research opportunity and supporting me in many ways. The most important thing in PhD life should be stable funding status. In this regard, I have never been worried about the money so that I could focus on my thesis solely.

I would also thank to my thesis committee members. You provided me priceless comments on my research. Especially, Dr. Seung Soon Jang encouraged me a lot to me who was sometimes discouraged on my research. Your just one word made me confidence. And you led me here. Thank you so much.

To Camellia Henry. You are the person who helped me when I transferred from precious school. You always responded quickly regarding my questions. I was able to concentrate on my research, not spending many times on something other than research.

Finally, I would like to thank to GT system, such as OIE, OIT, and Marcus nanotechnology building staffs. Your well-established system also made me to focus on my research.

Again, I thank to people surrounding me. I could not have done this in 3 years without you.

TABLE OF CONTENTS

LIST OF FIGURES

LIST OF SYMBOLS AND ABBREVIATIONS

HDL	High-density lipoprotein
CVD	Cardiovascular disease
CAD	Coronary artery disease
rHDL	Reconstituted HDL
MD	Molecular dynamics
CG	Coarse-grained
AA	All atom
RCT	Reverse cholesterol transport
apoA1	Apolipoprotein A1
eHNP	Engineered HDL mimetic nanoparticle
eHNP-A1	apoA1 based eHNP
eHNP-r4F	r4F based eHNP
CE	Cholesteryl ester
PON1	Paraoxonase-1
SAA	Serum amyloid A
LDL	Low-density lipoprotein
HAPs	HDL-associated proteins
DMPC	Dipalmitoylphosphatidylcholine
ABC	ATP-binding cassette
ABCA1	ABC transport A1
LCAT	Lecithin cholesterol acyltransferase
CETP	Cholesterol ester transfer protein
PLTP	Phospholipid transfer protein

SR-B1	Scavenger receptor B1
LJ	Lennard-Jones
RMSD	Root mean square deviation
RT	Room temperature

SUMMARY

High-density lipoprotein (HDL) is an endogenous biological molecule with high heterogeneity, playing critical roles in several biological events including anti-inflammation and lipid homeostasis. However, it is difficult to uncover the detailed structural and biological function of each HDL component, mainly due to the heterogeneity of HDL induced by multiple compositions and HDL-associated proteins. To overcome heterogeneous characteristics of HDL, reconstituted HDL (rHDL) form has been presented to synthesize simplified form of HDL with major components in HDL, such as apolipoprotein A1 (apoA1), phospholipids (PL), and free cholesterol (FC). Recent developments in microfluidics have allowed us to produce more homogeneous HDL-mimetic nanoparticles with higher reproducibility. In addition, computational approaches have been introduced to conduct structural analysis of nanoparticles along with the development of computational methods.

we introduce a computational strategy of molecular dynamic (MD) simulation with experimental correlations. Coarse grained (CG) MD simulation enables the detailed prediction of the HDL-mimetic nanoparticle's structure, and binding structure of HDL with a major HDL associated proteins (HAPs), paraoxonase1 (PON1), while the microfluidic platform leads compositionally homogeneous nanoparticle synthesis to validate computational results. Our approach provides an insight to precisely analyze the compositionally and functionally heterogenous HDL and can be applied to elucidate the detailed binding mechanism of other associated proteins on well-defined HDL.

CHAPTER 1. INTRODUCTION

1.1 Background

1.1.1 High-density lipoprotein

High-density lipoprotein (HDL) is a natural multifunctional nanoparticle that plays important roles in terms that it has been known to transport cholesterol lipids from peripheral tissues to the liver, which is called reverse cholesterol transport (RCT) [2-4]. HDL is nano-sized particle that exists in various forms (discoidal and spherical) regarding its heterogeneous compositions [5-8]. Apolipoprotein A1 (apoA1, 243 amino acids) [9], major protein in HDL, is secreted ma inly from the liver in the lipid-poor or lipid-free form. And the apoA1 becomes lipid-bound state by uptake of free cholesterols and phospholipids from plasma membrane mediated by ATP-binding cassette (ABC) transporter A1 (ABCA1) [10, 11], resulting in the formation of discoidal shape (nascent HDL) [12]. These discoidal particles are composed of phospholipids bilayer with amphiphilic cholesterol and apoA1s encircle outer perimeter of lipids with double-belt like conformation [13-15]. After lecithin cholesterol acyltransferase (LCAT) esterifies cholesterol in lipid bilayer [16, 17], cholesteryl esters (CEs) move from the lipid bilayer surface to the hydrophobic core of HDL, transforming discoidal shape to spherical conformation. Also, HDLs undergo dynamic compositional changes by interacting with lipid transfer proteins, such as cholesteryl ester transfer protein (CETP) and phospholipid transfer protein (PLTP), becoming large size sphere [18]. Then, HDLs transport CEs to the liver mediated by scavenger receptor B1 (SR-B1), which selectively takes up lipids[19-21]. During this dynamic remodeling of HDLs, an imbalance between the amphipathic surface and

hydrophobic core may be possible reason that HDL size becomes large with three to four apoA1 molecules [22].

1.1.2 Heterogeneous property of HDL

One important reason to study HDL is because HDL has long been believed to be a therapeutic promise [23] due to the fact that plasma HDL levels have inverse association with cardiovascular disease (CVD), which is top cause of death in U.S. [24, 25]. However, in recent clinical studies, raising plasma HDL levels failed to demonstrate reduced CVD events in patients with coronary artery disease (CAD) [26], possibly due to dysfunctional HDL nanoparticles that no longer have the long-believed atheroprotective function [27]. In fact, it has been demonstrated that HDL components are dynamically modified during a number of biological processes, generating a heterogeneous population of HDL and inducing altered endothelial effects of HDL. For example, paraoxonase-1 (PON1), an enzyme of HDL, contributes to the anti-atherogenic function of HDL [28-31] whereas HDL-bound serum amyloid A (SAA) becomes pro-inflammatory [32-35]. Due to the overwhelming number of HDL components, however, the mechanisms of the altered effects remain poorly understood [36, 37].

1.1.3 Reconstituted HDL

Despite of heterogeneous characteristic of HDL, most current studies inevitably rely on bare measurement of in vivo plasma level of HDL and associated proteins. The heterogeneous properties of which result in high variations and low reproducibility restricting mechanistic studies on HDL functions. To overcome these challenges, reconstituted HDL (rHDL) has been developed to study the structural and biological

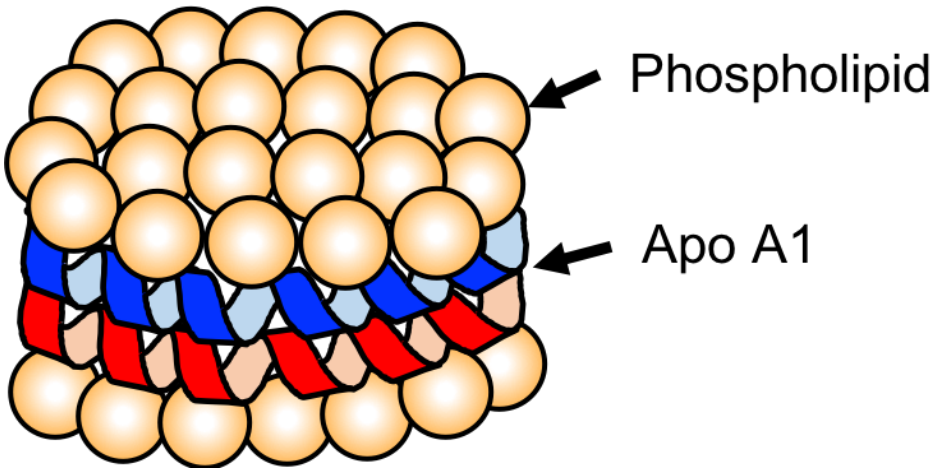

Figure 1. reconstitute HDL with major components of HDL (two apoA1s and DMPCs)

functions of HDL [38-41]. We showed a microfluidic synthesis technology that allowed us to enhance HDL synthesis reproducibility and particle homogeneity [42, 43], and were recently able to detect the distinct biological function and drug delivery performance of two different engineered HDL-mimetic nanoparticles (eHNPs) in vitro and in vivo [44]. This integrated approach has provided a better understanding of the biological roles of apolipoprotein A1 (apoA1), the scaffold protein of HDL that has important biological roles [45-48], and the mimetic peptide r4F in a mechanistic manner, with potential to investigate the biological roles of a variety of HDL functional components. However, it would be inefficient to experimentally study the functions of a number of HDL components and it remains unclear how these elements interact with HDL for the specific biological functions

1.1.4 Molecular dynamics simulation on HDL

Meanwhile, computational approaches using molecular dynamics (MD) simulations have been applied for a better fundamental understanding of structural dynamics of HDL [49]. The scaffold protein, apoA1, of discoidal HDL has been comprehensively investigated

using MD simulations over the last two decades. Applying theoretically and experimentally proposed apoA1 structures, such as double-belt, picket fence, and hairpin model, on MD computations, the most stable (low potential energy comparing to others) apoA1 structure, double-belt model, has been proposed among them. Then, this double-belt conformation of apoA1 has been widely accepted for discoidal HDL [50-55]. Efficient coarse-grained (CG) forcefield [56, 57] has successfully simulated the disassembly and morphological transition (discoidal to spherical) of rHDL [58-60]. While there have been extensive studies of structural analysis of discoidal HDL, much less is known about the apoA1 structure in spherical HDLs. They contain CEs and triglycerides in hydrophobic core, encapsulated by amphipathic phospholipids and cholesterol surface. Despite of a few published reports regarding spherical HDL experimentally, trefoil apoA1 model has been proposed with cross-linking chemistry with mass spectrometry (MS) [48]. However, this topic is still understudied. In addition, even though there have been comprehensive studies of structural and biological functions of HDL, little is known about the relations between HDL and its associated elements responsible for HDL functions. For example, paraoxonase-1 (PON1) promotes cholesterol efflux and inhibits low-density lipoprotein (LDL) oxidation [61, 62]. However, it remains unclear how PON1 interacts with HDL and how the interactions alter the biological functions of HDL.

1.2 Molecular dynamics simulation

Since 1970s, MD simulations have applied to biological system, solving equation of motion for the atoms. The results provided diffusive characteristics of atom motions [63]. Since then, MD simulation approach to biological studies has grown rapidly, as development of MD simulation code itself along with the rising performance of computer

hardware. The exponential increase of manuscripts related to MD simulation is clear as searching the number of publications with the keywords, “molecular dynamics” [1]. This trend shows clear importance of MD simulation for predicting the function of molecules, and discovering the mechanisms underlying functions depending on a complete understanding of biological molecules, including their dynamics.

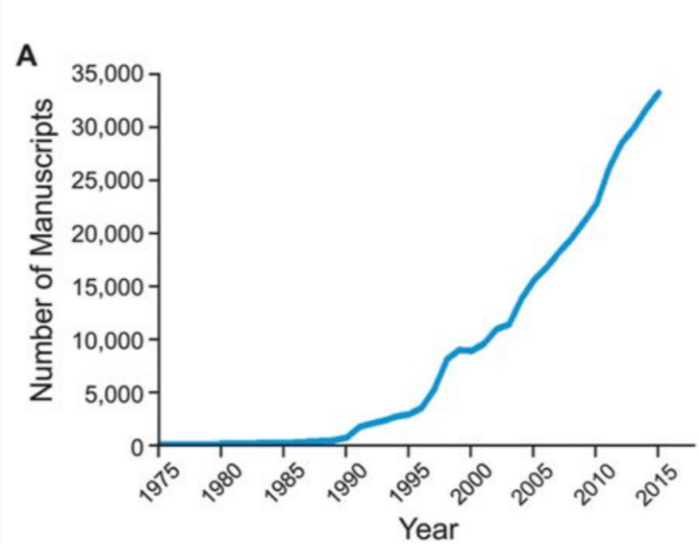

Figure 2. The exponential increase of MD simulation approach [1]. This work is licensed under the Creative Commons Attribution 4.0 International License.

1.2.1 Basic knowledge of MD simulation

MD simulation calculates Newton’s second law of motion numerically to determine the trajectory of atoms and molecules.

$$\boldsymbol{F} = \boldsymbol{ma} \qquad (1)$$

, where F is force on an atom, m is mass of the atom, and a is the acceleration of atom. And F(r) can be expressed by potential energy function regarding coordinates of all atoms, U(r).

$$\boldsymbol{F(r) = -\nabla U(r)} \quad (2)$$

Then,

$$\boldsymbol{dv/dt = F(r)/m} \quad (3)$$

$$\boldsymbol{dr/dt = v} \quad (4)$$

Those two derivatives are solved by numerical integrations. And Potential energy U(r) is combined with bonded interactions (bonds, bend angles, torsion angles) and non-bonded interaction (Lennard-Jones: van der Waals, Coulomb: electrostatic).

$$\boldsymbol{U(r) = U_{bonds} + U_{bend\ angles} + U_{torsion\ angles} + U_{LJ} + U_{Coulomb}} \quad (5)$$

1.2.1.1 Non-bonded interactions

Force fields divide non-bonded potential into two Van der Waals and electrostatic interactions.

Lennard-Jones (LJ) potential (Van der Waals):

$$U_{LJ}(r) = 4\varepsilon[(\sigma/r)^{12} - (\sigma/r)^{6}] \quad (6)$$

ε indicates the strength of the interaction and σ is a length scale. Both parameters are

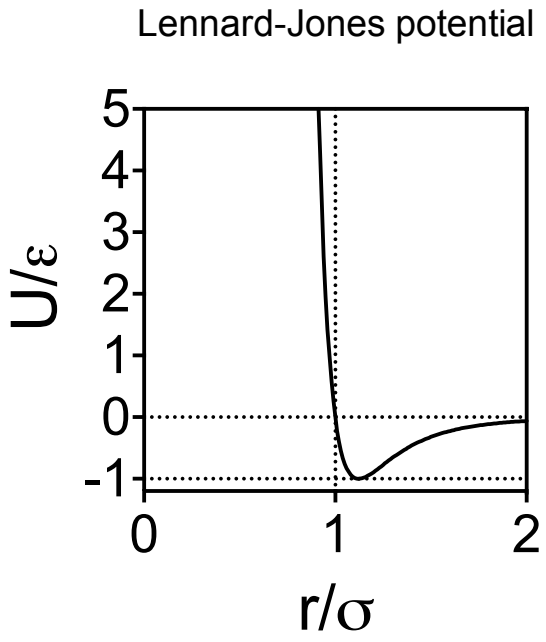

Figure 3. Lennard-Jones potential graph (Strength v.s. distance)

chosen regarding particular properties of the system. LJ potential shows strong repulsive force when r is less than σ ($\left(\frac{\sigma}{r}\right)^{12}$: repulsive term) due to overlapping electron orbitals. On the other hand, attraction force is the maximum when r ≈1.122 σ.

Coulomb potential (electrostatic):

$$U_{coulomb}(r) = Q_1Q_2/4\pi\epsilon_0 r \quad (7)$$

Comparing to the molecule distance, r in LJ potential, Coulomb potential is less sensitive in the distance, and it indicates very long-range potential comparing to LJ potential.

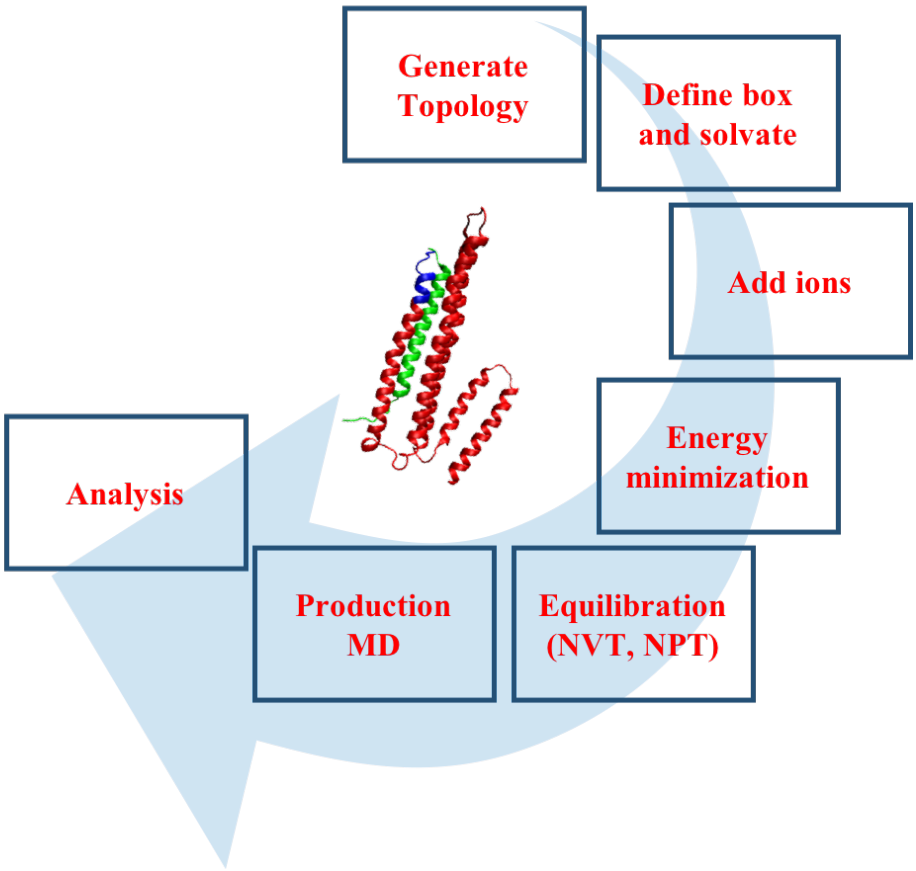

Figure 4. General molecular dynamics simulation flow chart

1.2.2 MD simulation flow chart

General MD simulation flow is shown in above figure. Basically, a molecule structure, that we want to simulate, is mandatory for sure. And we need specific force fields regarding

what we want to solve. Then a simulation topology file can be generated in GROMACS. The most important thing to consider in entire simulation process is to set up the simulation box size. Large size simulation box contains many molecules such as water and ions, then simulation time will rise exponentially. Molecule fitted box size may arise a problem. Because each box faces are set as periodic boundary condition, the molecule sometimes cross a box face, interacting with other side of the molecule. So, it is critical to set up the optimal size of simulation box. In the box, designated molecules, water molecules, and ions are located. Before the actual simulation, the structures in the system should be relaxed through the process called energy minimization. Then, equilibration of solvent and ions around molecule structure is needed to set designated temperature and pressure, and to avoid system collision. After two equilibration processes, it is ready to implement MD simulation. After this whole process, several resulting files are generated and those are used for further analysis.

1.2.3 Coarse-grained model (MARTINI force field)

Coarse-grained (CG) MD simulation model has been developed to analyze the dynamics of large size molecules. Although it is inevitably true that CG MD simulation loses its

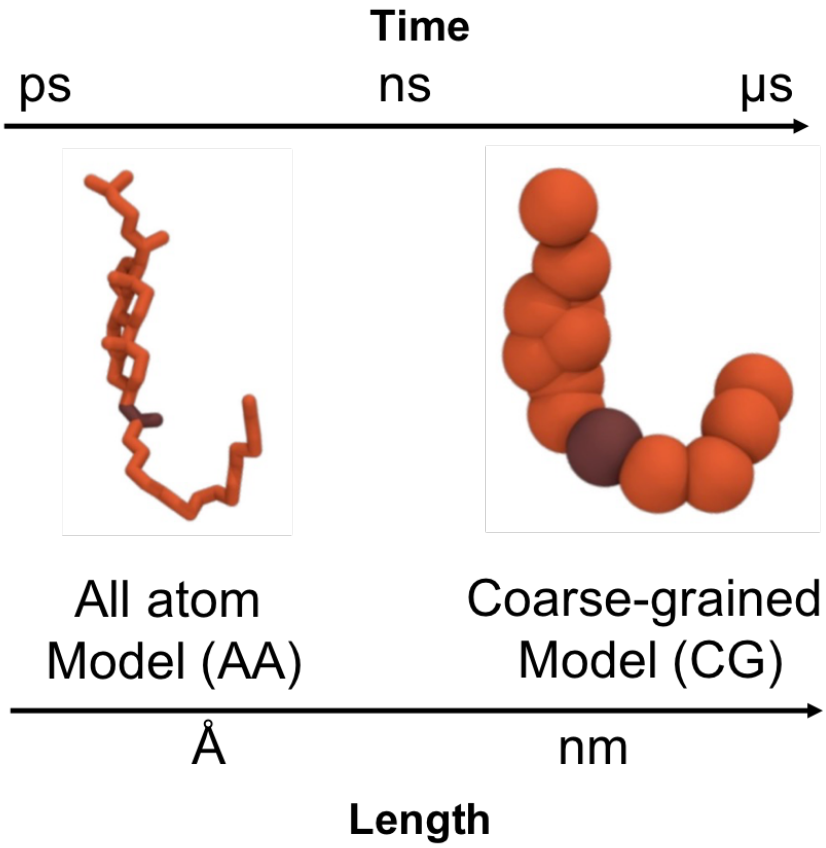

Figure 5. Comparison between all atom and coarse-grained model

accuracy comparing to all atom (AA) model by modeling 4 atoms into 1 big bead (four-to-one mapping), it enlarges time and length scale of the system. Currently, CG MD simulation is used to predict the tertiary structure, maintaining secondary structure, which is one limitation to be solved as a future research. As each force field has their own purpose to calculate, MARTINI force field is specialized to compute the interaction between lipid membrane and proteins, and this force field is used in a number of publications showing its reliability.

1.2.4 Software packages

There are several MD simulation open source codes. They have their own particular force fields to solve molecular interaction, which is the reason to simulate. Remarkably, the use of GROMACS and LAMMPS are growing exponentially, although the Figure 6 does not show clear explanations because many publications do not cite software. Visual molecular dynamics (VMD) is tool to visualize and analyse resulting molecule structures. These increasing number of citations of computational approaches to biological system investigations explicitly indicates how this computational method is important.

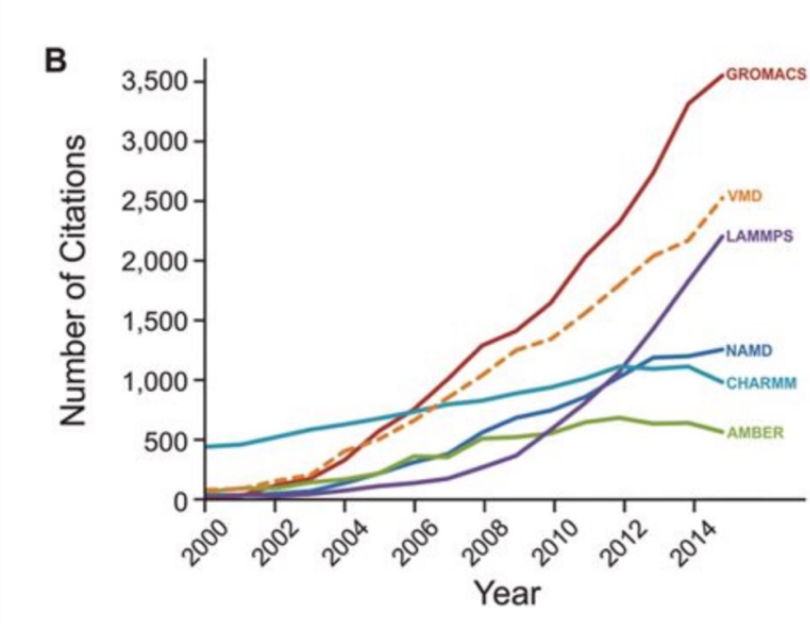

Figure 6. MD simulation software packages regarding the number of citations [1]. This work is licensed under the Creative Commons Attribution 4.0 International License.

GROMACS stands for GROningen Machine for Chemical Simulation, developed in the Biophysical Chemistry of university of Groningen. The algorithm that they adopt enables faster simulation time than many simulation programs. And it is supported by different force fields, which makes GROMACS very flexible. Besides, MARTINI force field is compatible to GROMACS.

In my research, I adopt GROMACS molecular dynamics package with advantages in terms of simulation speed, flexibility, extensive amount of information on the web (forum), and well-documented information in manual. And MARTINI force field is used for CG MD simulation, because it is specialized to conduct cell membrane and protein simulations which are related to my research. And it has a number of publications in high impact journal indicating its reliability. VMD is used as a molecular visualization program. It allows us to display, animating, and even analyzing biomolecular systems with 3-dimensional graphics.

1.3 Research objectives

The primary objective of our study is to expand our understanding in HDL-mimetic nanoparticle modeling with the CG MD simulation with experimental correlations. We chose to specifically study engineered HDL-mimetic nanoparticles (eHNPs), and one of HDL associated protein, paraoxonase-1 (PON1) to predict protein binding structure to eHNP. To achieve our primary objective, the study is divided into the following aims:

1. Apply a coarse-grained molecular dynamics simulation approach to model the structure of apolipoprotein A1 based HDL-mimetic nanoparticles (eHNP-A1).

2. Apply a coarse-grained molecular dynamics simulation approach to model the structure of r4F peptide-based HDL-mimetic nanoparticles (eHNP-r4F) with direct comparison to eHNP-A1
3. Investigate preferable PON1 binding structure to eHNPs and its binding mechanism

CHAPTER 2. COMPUTATIONAL MODELING OF APOLIPOPROTEIN A1 BASED HDL-MIMETIC NANOPARTICLE FOR STRUCTURAL ANALYSIS

2.1 Background

2.1.1 Double-belt structure of apoA1 in nascent HDL

As CG MD simulation codes have been developed along with the performance of computer processors, it enables large size and complex molecules analysis faster than conventional AA model. This computational approach has been used to investigate HDL nanoparticle structure in biological system. To avoid compositional complexity of HDL, nanoparticles have been designed to simplified form, named nanodiscs with major components in HDL, apoA1 and phospholipids. Initial nanodisc model has 1:80 molar ratio (apoA1: DMPC), because experimentally well-known structure has the ratio at earlier time when nanodisc researches were initiated [64, 65]. And initial studies were of interest in apoA1 structure in HDL, due to the biologically functional importance of apoA1 in HDL, and apoA1 structure is still not clearly uncovered. However, apoA1 structure in nascent HDL has been extensively studied computationally, suggesting that HDL with double-belt like apoA1 showed stable energy status among other proposed models, such as picket fence and hairpin model. Besides, shape transition from discoidal to spheroidal HDL has been studied by incorporating 60 mole of hydrophobic cholesteryl ester (CE) molecules without any structural change in apoA1 [58]. This provided possible CE molecules incorporating mechanism, showing shape transition.

2.1.2 Trefoil model of apoA1 in spherical HDL

While the apoA1 structure in discoidal HDL has been comprehensively explored, much less is studied about the apoA1 structure in spherical HDL [48, 66, 67]. Spherical HDL contains triglyceride and CE molecules in the hydrophobic core, and those hydrophobic molecules are surrounded by amphipathic phospholipid and cholesterol monolayer. The reason why the apoA1 structure in spherical HDL is important is that the activity of HDL remodeling factors such as LCAT [45] and CETP [68] might be affected by HDL nanoparticle shape. Trefoil apoA1 model was first proposed by cross-linking chemistry with mass spectrometry (MS). Both discoidal and spherical HDL show similarity in general structural organization of apoA1, and cross-linking pattern was explained in human plasma HDL. However, few publications have experimentally demonstrated spherical HDL, and computational approach has never been applied for this model.

Here, I reproduce double-belt apoA1 configured HDL-mimetic nanoparticle with experimental correlation to confirm validity of CG MD simulation model, which is critical step for computational reliability. Then, I investigate both double-belt and trefoil apoA1 structure in spherical HDL.

2.2 Results

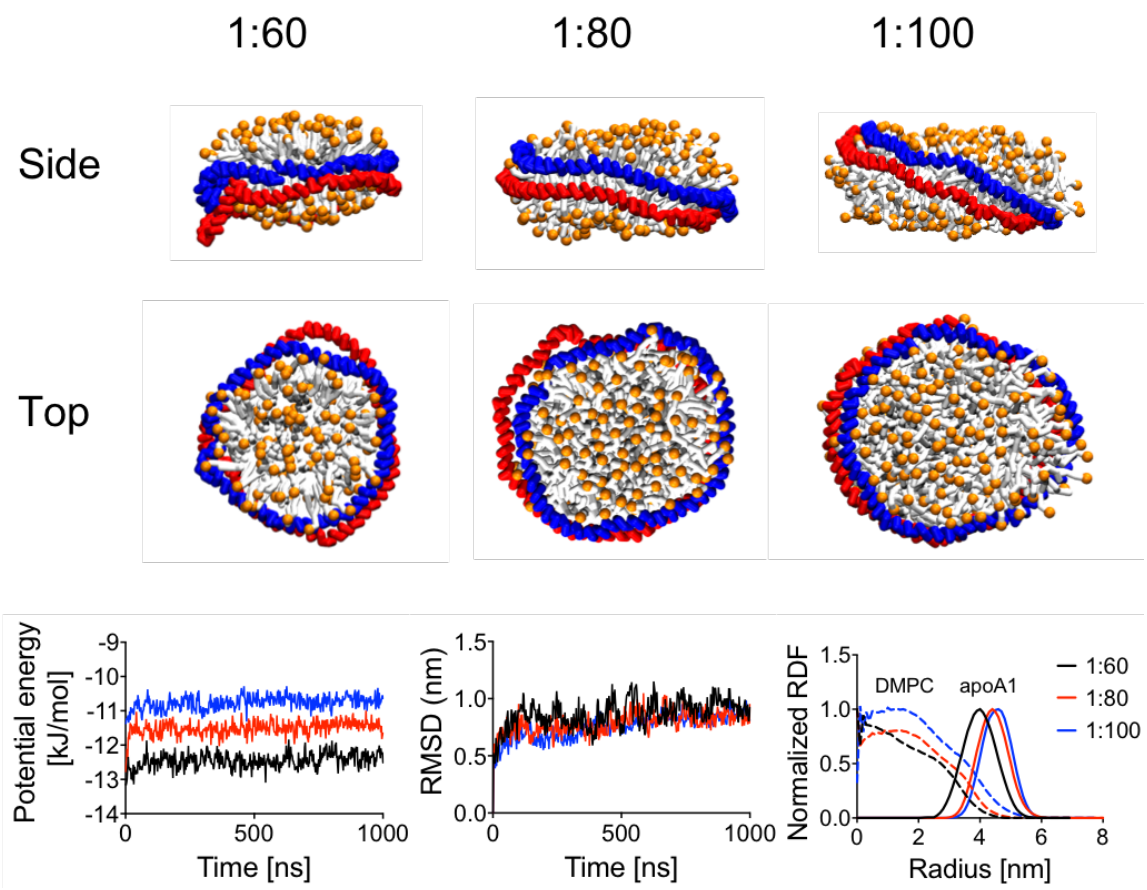

Figure 7. Energy and structural comparison among three different ratios

2.2.1 Modeling engineered HDL-mimetic nanoparticles with different ratio

CG MD simulation was performed to reproduce and explore the structure of rHDL. MARTINI force field [56] was used as CG model, because it is well-known for cell membrane and protein simulation with a number of publications. First, three discoidal rHDL models have been simulated to prove the structural differences and energy status. They have different apoA1 and DMPC ratio, which are 1:60, 1:80, and 1:100. Those ratios were selected within the range of nascent discoidal HDL from blood plasma [6]. Initially,

lipid bilayer and apoA1 double-belt model was used to reduce the simulation time, assuming final structure as disc type nanoparticle. This is because many studies about final structure of nanodiscs have been discusses. Those simulations were to validate simulation setup with the results from robust microfluidic nanoparticle synthesis. And 1:80 composition is the ratio that has been widely used in nanodiscs research, because this ratio was well documented from experiment at that time when nanodiscs research was initiated [64, 65]. I set up this simulation conditions based on the past report [69], which is lastest publication of CG MD simulation with MARTINI force field. I implemented simulation for 1000 ns which was enough, as other researches did for 500 ns. Over the simulation time, three nanodiscs with different composition kept their structures, and apoA1 structure maintained double-belt shape, as we expected. Among them, 1:60 ratio shows the lowest potential energy, which indicates stability of nanodiac. 1:100 ratio is still structurally stable, but relatively less stable than 1:60 case. This makes sense, because the distance among molecules are too short which has repulsion force, as demonstrated in LJ potential graph. As well as potential energy, root mean square deviation (RMSD) is another factor to explain the stability of molecule structure. RMSD of apoA1 for three simulations shows no significant differences, which means apoA1 structure stably encircled DMPC bilayer. In addition, due to the marginal location of double-belted-apoA1s, the radius of apoA1-ring gradually increased as the composition changed from 1:60 to 1:80, and saturated at 1:100 composition, suggesting that the size of HDL nanoparticle is confined by the dimension of apoA1.

2.2.2 Computational model validation with experimental correlation

To evaluate our simulation model by comparison with experimental results, we implemented our microfluidic technology to synthesize well-defined and highly homogenous HDL-mimetic nanoparticle comprising apoA1 and DMPC (engineered HDL-mimetic nanoparticle-A1; eHNP-A1), which led a composition of 1:73 mole ratio of apoA1 to DMPC [44]. The synthesized eHNP-A1 was highly homogenous shown in size distribution in dynamic light scattering (DLS), and well correlated with our simulation model as well as physiological pre-beta HDL as shown in transmission electron microscopy (TEM), possessing a discoidal shape with a 10 nm of diameter. The correlation of our simulation model with the microfluidically synthesized eHNP-A1 confirms the reliability and physiologically relevance of our model for further analysis.

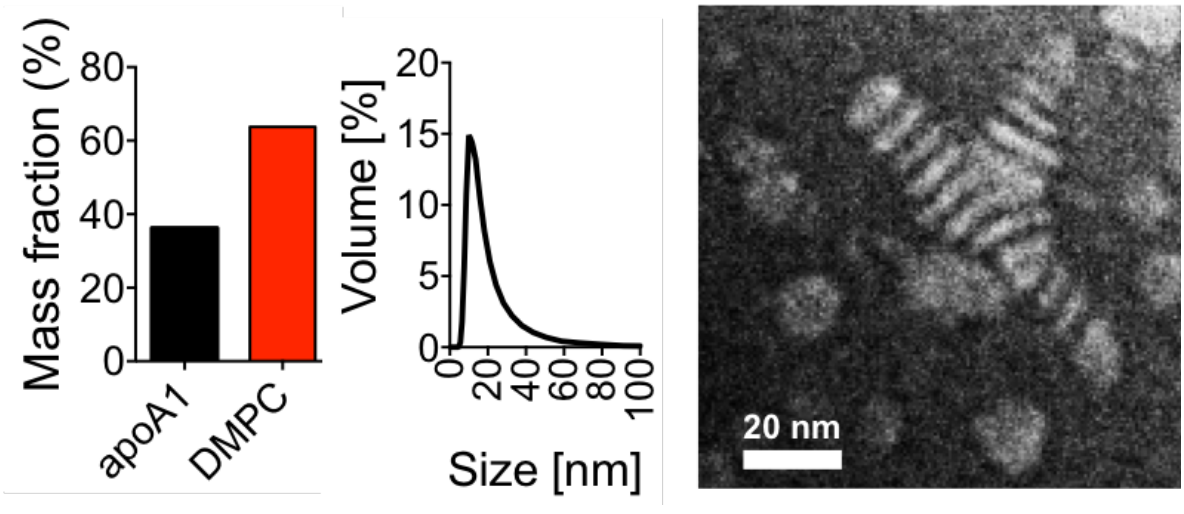

Figure 8. Experimental correlation with microfluidic synthesis

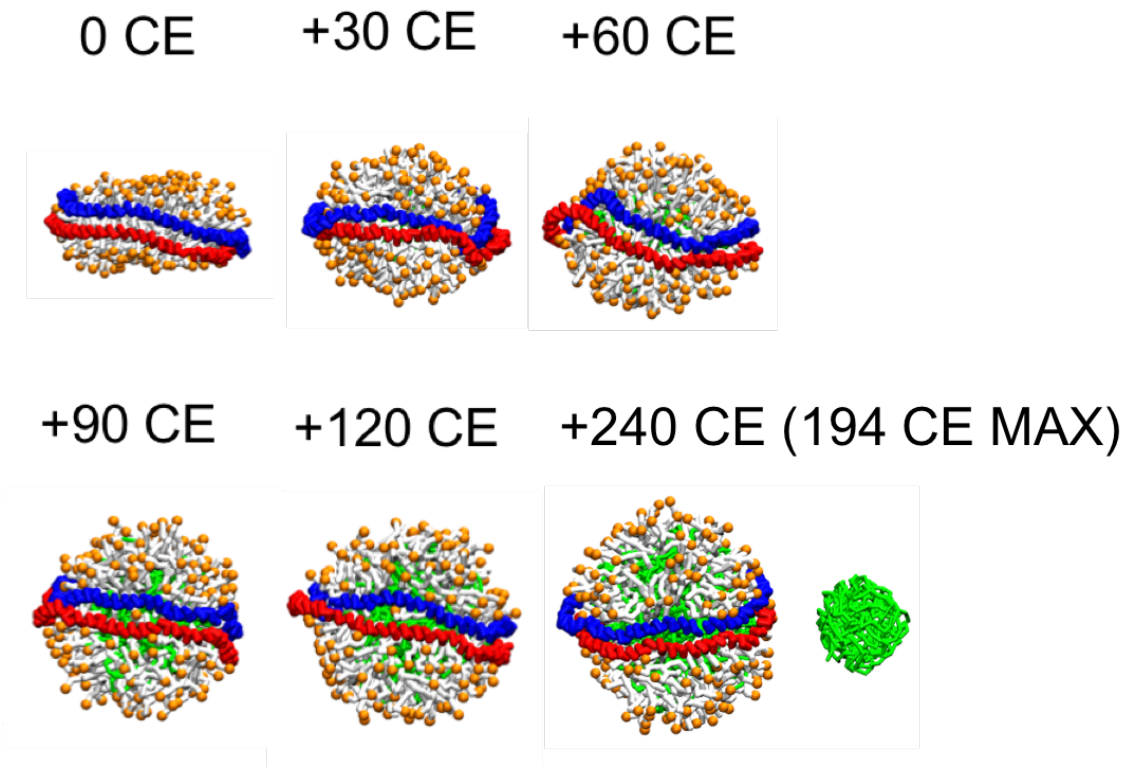

Figure 9. Shape transition from discoidal to spherical by incorporating CE molecules

2.2.3 Shape transition and loading capacity

Although previous research showed shape transition from discoidal nanodiscs, only 60 number of CE molecules were added in the simulation system to see maturation of HDL. However, matured HDL from blood plasma contains more hydrophobic lipids, such as triglycerides and CEs in the core of HDL. So, it is important to know (1) how many hydrophobic molecules can be incorporated in double-belt configured discoidal nanodiscs, also (2) if structural change affects the structure of double-belt apoA1. To explore shape transition of nanoparticle, the number of CE molecules have been gradually added to discoidal eHNP-A1 in the system. As previous report has showed [shih], discoidal eHNP-A1 transformed to spheroidal shape until adding 60 CE molecules. Until adding 120 CE

molecules, eHNP-A1 incorporated with them, transforming to spherical shape. However, 240CE molecules were not completely inside of eHNP-A1. 46 CE molecules were found outside of eHNP-A1, aggregating each other. Total 194CE molecules can be incorporated in 1:80 discoidal eHNP-A1. In addition, radial distribution function (RDF) analysis demonstrated no significant size changes while transforming the shape. It proposes double-belt apoA1 structure maintains initial 1:80 discoidal eHNP-A1 size. Additionally, apoA1 double-belt structure was not affected by simply adding hydrophobic molecules.

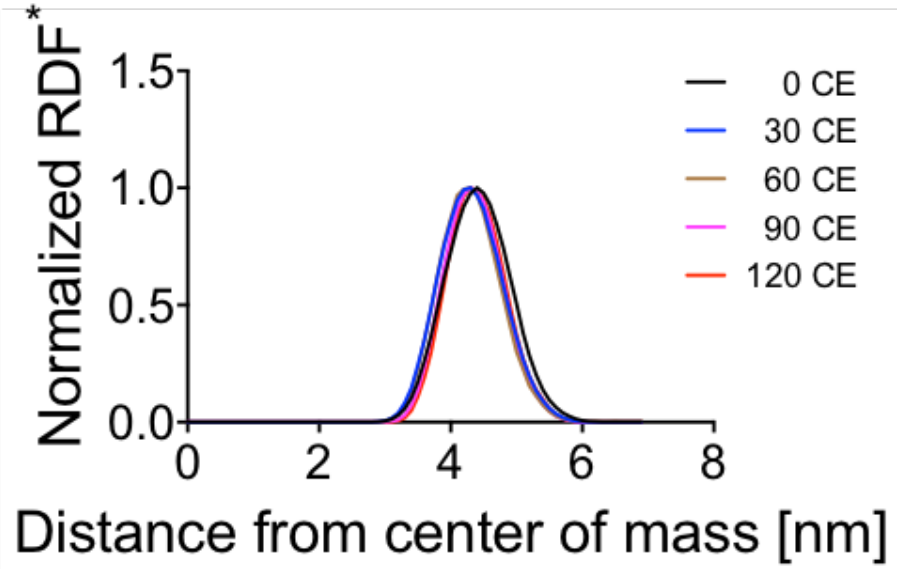

Figure 10. Diameter comparison among different CE contained nanoparticles

2.2.4 apoA1 structural analysis of trefoil in spherical HDL

Generally, it is impossible to form discoidal shape with trefoil apoA1 configuration. So, initially, 90 CE molecules were added into the nanoparticle which has already been

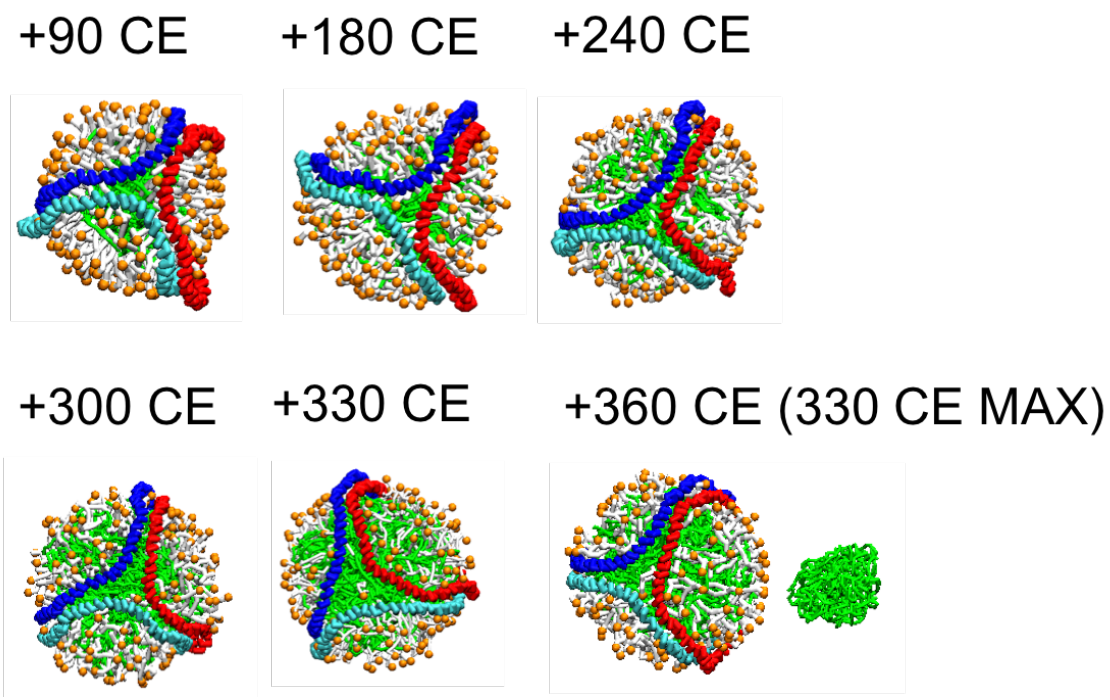

Figure 11. CE molecules incorporation to trefoil configured apoA1 based nanoparticle

modeled with 1:80 discoidal eHNP-A1 and replaced from double-belt to trefoil apoA1 to explore apoA1 structural change from trefoil form. Like previous double-belt case, the number of CE molecules were gradually increased in the system. With trefoil apoA1 configuration, 330 CE molecules were found inside of hydrophobic core of eHNP-A1, while 30 CE molecules were aggregated outside and were not involved in the nanoparticle. Comparing to double-belt eHNP-A1 case, trefoil structured eHNP-A1 can contains more hydrophobic molecules inside of nanoparticle, as maximum 330 CE molecules. This result supports the existence of larger size HDL in blood plasma with 3-5 molecules of apoA1. Besides, trefoil apoA1 structure also stabilize spherical nanoparticle structure, keeping its size.

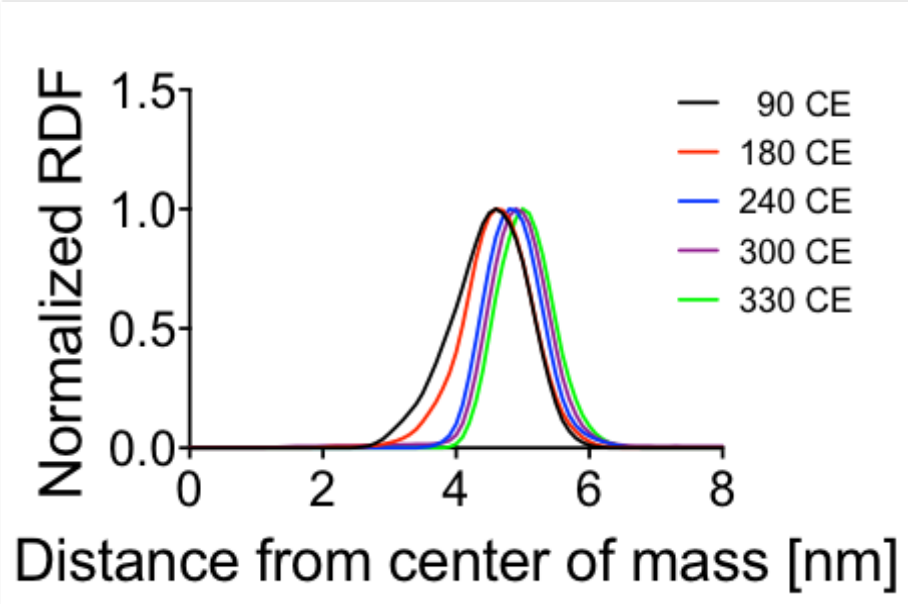

Figure 12. Diameter comparison among different CE contained nanoparticle for trefoil configured nanoparticle

2.3 Conclusion

I successfully applied CG MD simulation and reproduced discoidal shaped HDL-mimetic nanoparticles, as well as validating with experimental correlations. As well as this, I was able to model and synthesize physiologically relevant to human plasma HDL. This validated MD simulation configuration has been applied to uncover currently unsolved biological questions regarding HDL structure. From these simulations, we have come to know the structural roles of apoA1. Both double belt and trefoil apoA1 models limit the size of nanoparticles, stabilizing the form of nanoparticles. Also, the increase in the size with three apoA1 molecules may explain the large size HDL existence with 3-5 number of apoA1 in blood plasma.

2.4 Methods

2.4.1 MD simulation

GROMACS 4.5.7 [70] was used as MD simulation software package with MARTINI force field [56] in conjunction with ElNeDyn[57] to maintain secondary and tertiary structure. Double-belt apoA1 structure was obtained from CHARMM-GUI [71, 72]. DMPC molecules were used as phospholipid. For 3 simulation cases, 120, 160, and 200 number of DMPC bilayer molecules were located inside of double belt apoA1 in 15 x 15 x 15 x nm sized simulation box, as an initial configuration. The system was solvated with water molecules and neutralized with Na^+ counterions. Then, this system was energy minimized with steepest descent algorithm for 5000 steps. Next, equilibrium step was performed with molecule restraints. Simulation time step, 20 fs was set up, which is proper range in MARTINI force field. Total simulation time, 1000 ns was set for all simulations. Temperature kept 298K for RT.

2.4.2 eHNP synthesis

A three-inlet microfluidic device that generates propagating microvertices was used for a single-step self-assembly of eHNP-A1 according to the previous report with slight modification [44]. In brief, 1,2-dimyristoyl-sn-glycero-3-phosphocholine (DMPC, Avanti Polar Lipids, AL; 2.75 mg/mL) in absolute ethanol was introduced into the center inlet of the microfluidic device at a flow rate of 0.8 mL/min. Apolipoprotein A1 (Millipore Sigma, MA; 0.2 mg/mL) in phosphate buffered saline (PBS, pH = 7.4) was introduced into two

outer inlets at a flow rate of 2.2 mL/min. Each of DMPC and apoA1 solution was homogenously injected using a programmable syringe pump (Harvard Apparatus, MA) at the desired flow rates. After running the syringe pump, the mixture solution was collected from outlet, followed by transferring the solution to centrifugal membrane filter (EMD Millipore, Germany) with a molecular weight cut off (MWCO) of 50,000, and purified 5 times in PBS at a speed of 3900 rpm for 30 min. Synthesized eHNP-A1 was stored at 4^{o}C for further modification.

2.4.3 eHNP characterization

Hydrodynamic volume of eHNP-A1 was obtained by a Zetasizer Nano (Malvern Instrument, Malvern, UK). For the monitoring of size and morphology of eHNP-A1, negatively stained samples were observed using a transmission electron microscope (TEM; Hitachi 7700, Hitachi, Japan) at 120kV coupled with the Digital Micrograph camera and software suite from Gatan.

CHAPTER 3. COMPUTATIONAL MODELING OF R4F PEPTIDE BASED HDL-MIMETIC NANOPARTICLE WITH DIRECT COMPARISON TO APOA1 BASED HDL-MIMETIC NANOPARTICLE

3.1 Background

3.1.1 HDL mimetic nanoparticles with apoA1-mimetic peptides

Along with the engineering HDL-mimetic nanoparticles with precursors from blood plasma, various apoA1-mimetic peptides for synthetic form of HDL has been developed to target diseases, such as CVD and Alzheimer's disease (AD) [73, 74]. ApoA1 has 243 amino acids, and it is composed of 10 alpha helices. Comparing to apoA1 structure, apoA1-mimetic peptide are 18-22 amino acids with alpha helix structure. The main reason for use of apoA1-mimetic peptides is the cost. Comparing to apoA1, apoA1-mimetic peptides are cost-effective, and it does not need any purification and expensive tests to check infection and endotoxin free [75]. Among the studies regarding mimetic peptides, reverse-4F (r4F) has demonstrated the performance of drug delivery and atheroprotective role in mouse model [74, 76-79]. Engineered HDL-mimetic nanoparticle with r4F peptides has already shown HDL-like structure and biological relation to receptor B1, comparing to HDL. However, a direct comparison between r4F and apoA1 in HDL-mimetic nanoparticle (eHNP-r4F and eHNP-A1, respectively) form has never been studied. In this study, we apply combined approach to compare and analyze the structures between apoA1 and r4F in an HDL-mimetic nanoparticle, computationally and experimentally.

3.1.2 Structural difference between apoA1 and r4F peptide

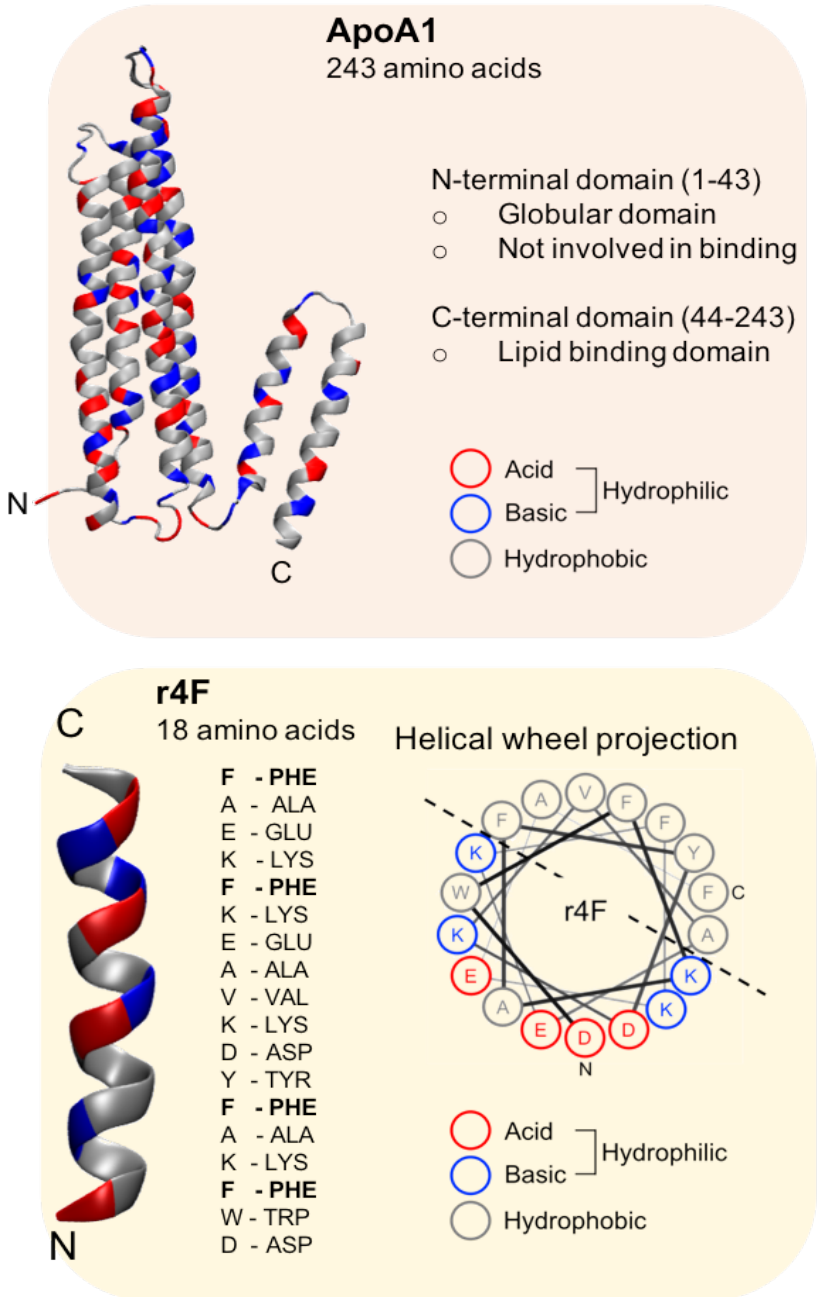

Figure 13. Structural differences between apoA1 and r4F peptide

apoA1 is a major protein component of HDL in human blood plasma, which is composed of 243 amino acids and 10 alpha helices. apoA1 stabilizes lipid membrane on the surface of an HDL particle, and is related to anti-inflammatory function of HDL. Comparing to apoA1, r4F peptide has 18 amino acids, which is much shorter than apoA1. And amino acid arrangement is designed on purpose that hydrophobic residues are located in one side of the helix. The purpose of this design is to cover hydrophobic tail of membrane lipids.

3.2 Results

3.2.1 HDL-mimetic nanoparticles comparison from microfluidic synthesis

We synthesized two types of HDL-mimetic nanoparticles with well-defined microfluidic synthesis platform. Resulting nanoparticles were physiologically relevant to nascent HDL, which are discoidal shape and closer to 10 nm. Both TEM images of eHNP-A1 and eHNP-r4F showed famous rouleaux shape (like stacks of coins), indicating discoidal shaped nanoparticle. And the average size of eHNP-A1 is 10.1 nm and eHNP-r4F is 11.7 nm.

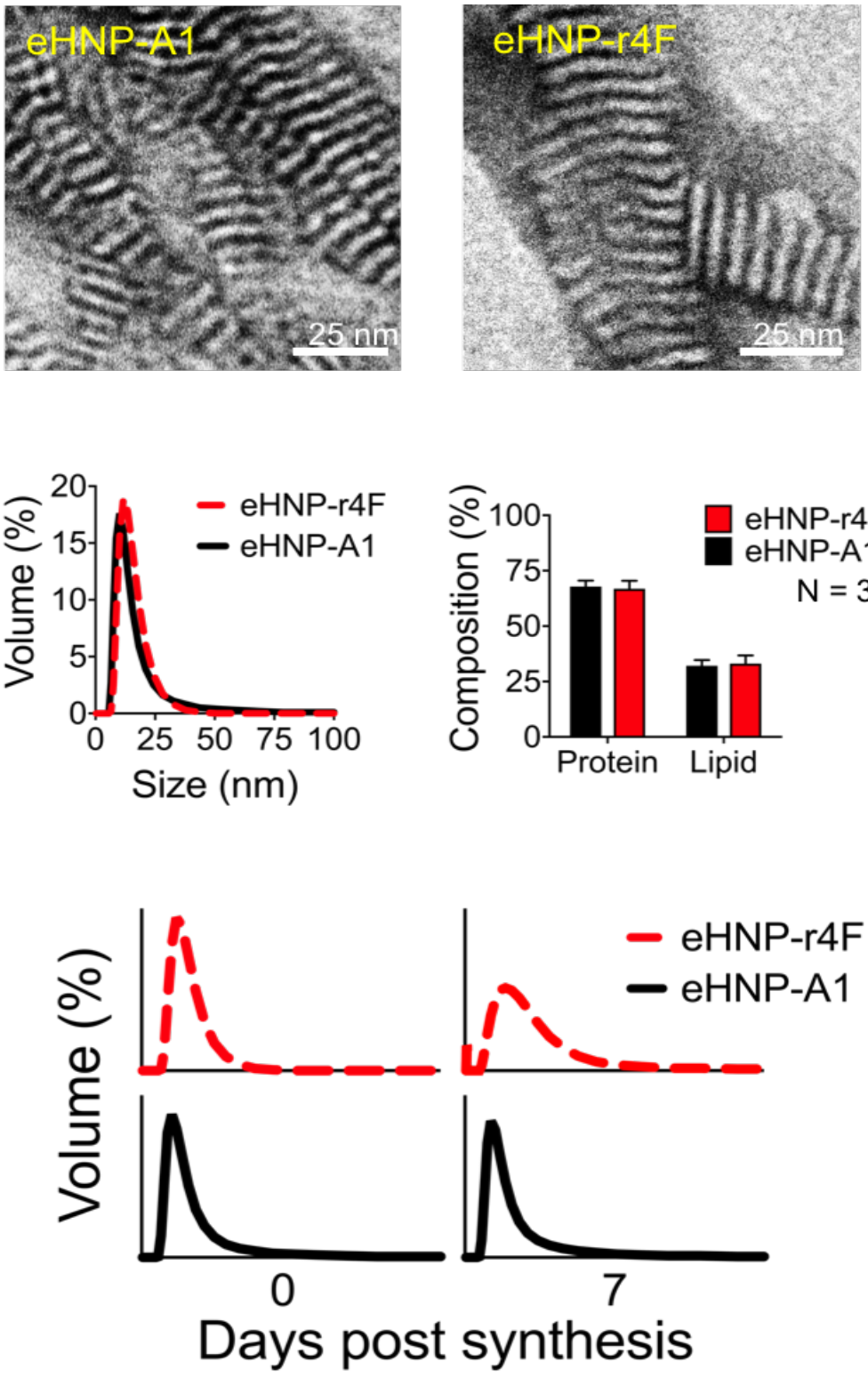

Figure 14. Characterization of eHNP-A1 and eHNP-r4F nanoparticle from microfluidic synthesis

Although there is slight size difference between them, DLS size distribution indicates that

both nanoparticles are almost similar in size and homogeneity. In addition, both had an almost identical protein-lipid composition. However, morphological difference was observed 7 days after particle synthesis. While eHNP-A1 kept their size and homogeneity, eHNP-r4F showed particle aggregation. This comparison explained the stability difference between both nanoparticles, and eHNP-r4F stability lower than eHNP-A1 particles. We hypothesized that r4F peptide could not cover hydrophobic tail of DMPC, then the hydrophobic region exposed to the hydrophilic solvent tried to find the hydrophobic region in other nanoparticles. Finally, eHNP-r4F particle aggregated over time.

3.2.2 Computational analysis of eHNP-r4F structure with CG MD simulation

CG MD simulations have been performed for structural analyses of both eHNP-A1 and eHNP-r4F. MD simulation enabled 1 to 1 nanoparticle comparison in molecular level. Not like eHNP-A1 simulation, eHNP-r4F simulation took a long time, because there was no assumption regarding final structures. Initially, total 1020 molecules (r4F: 60, DMPC: 960, [reference]) were located in 30 nm x 30 nm x 30 nm simulation box. Then, water and ions were filled in empty space in the box. This simulation went through 3.5 μs until small eHNP-r4F nanoparticles became one big particle after aggregation. For 1 to 1 comparison, eHNP-r4F which had similar size to eHNP-A1 was chosen. There was significant structural difference which may explain the low stability of eHNP-r4F. In both eHNPs, DMPC lipids

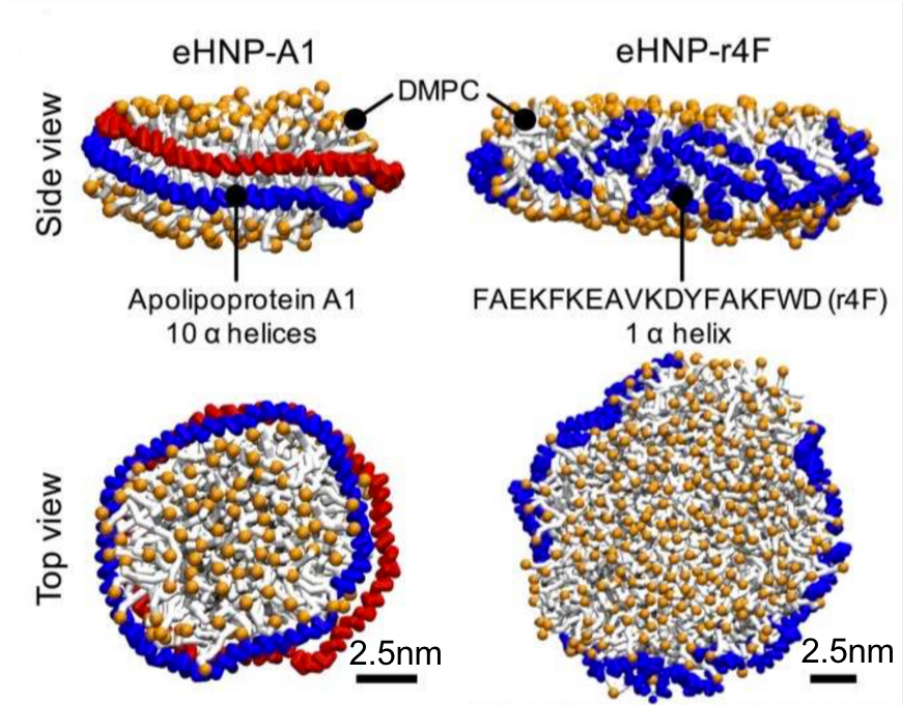

Figure 15. Structural comparison between eHNP-A1 and eHNP-A1 from MD simulation results

formed bilayer as expected. However, apoA1 played a membrane scaffolding role in nanoparticle structure, covering hydrophobic tail of DMPC, which would prevent particle aggregation with adjacent nanoparticles. On the other hand, hydrophobic region of DMPC in eHNP-r4F structure was exposed to hydrophilic solvent, which has possibilities to aggregate with other nanoparticles because of hydrophobicity. Consequently, r4F peptide formation in eHNP-r4F reduces particle stability having more chances to aggregate.

The view of entire simulation box would help to understand how eHNP-r4F is developing to one huge big particle. In initial configuration at 0 μs, each molecule was randomly distributed without any prediction of final structure. At 0.5 μs, 6 individual eHNP-r4Fs were seen, and r4F peptides were aggregated each other. Even, 3 particles in right hand side of simulation box, attached each other. Due to r4F peptides aggregation, hydrophobic tail of DMPC were opened to hydrophilic solvent, which led particle aggregation. Finally, several eHNP-r4Fs became one big particle. Even, some hydrophobic tail regions of DMPC were still exposed to water molecules, due to the lack of the number of r4F.

3.2.3 Structural differences of eHNP-r4F regarding different mole ratios

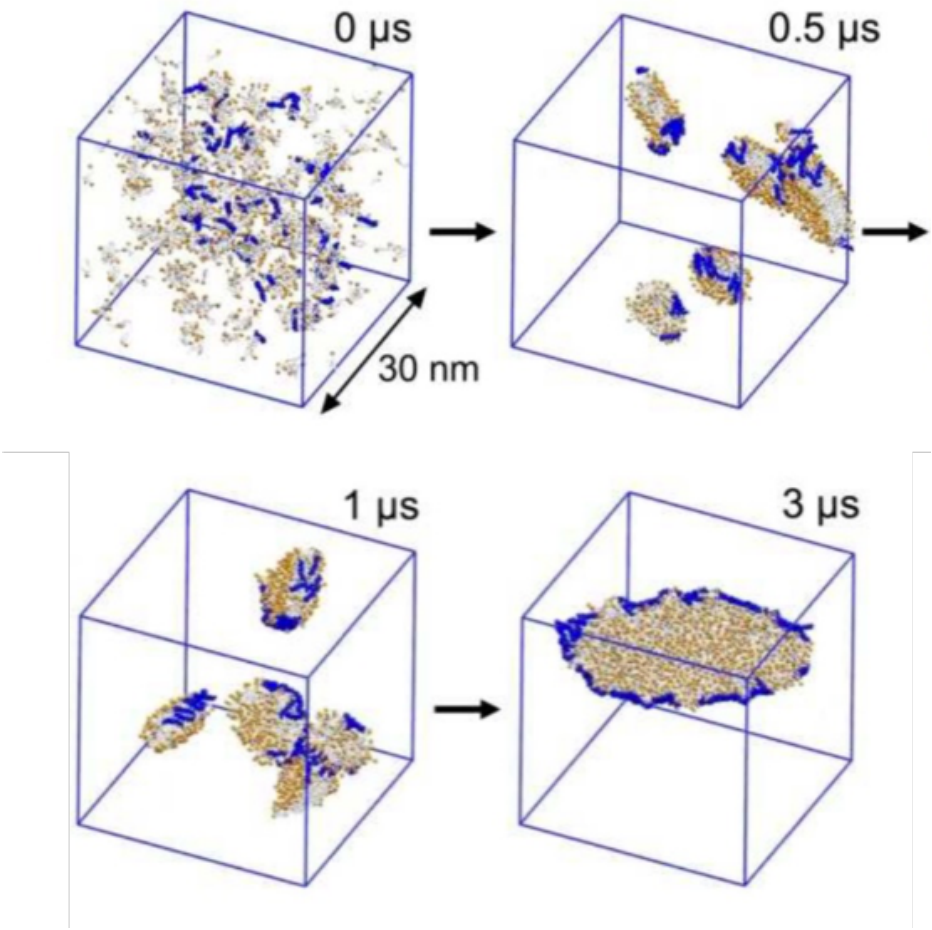

Figure 16. Nanoparticle aggregation over time

Main difficulty in eHNP-r4F synthesis is to cover whole hydrophobic tail of DMPC with r4F peptides, completely, as apoA1s do in HDL. One thing I could suggest with MD simulation was to increase the number of r4F peptide molecules to increase the possibilities to cover hydrophobic region, which would help to avoid particle aggregation. Three simulations were planned to suggest the best ratio to avoid aggregation by comparing each other (1:16, 1:8, 1:3, r4F: DMPC). From the results, although r4F peptide aggregation was inevitable, increasing the number of r4F peptide molecule helps to cover hydrophobic tail of DMPC, which may lead particle aggregation.

Ratio (r4F:DMPC)	1:16	1:8	1:3
Size (nm)	5.02/8.62	7.54/7.37	7.29/6.81/7.01
View 1	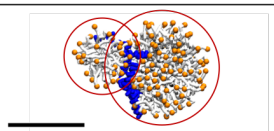	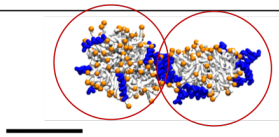	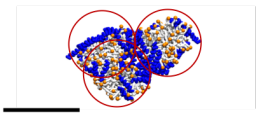
View 2	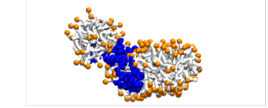	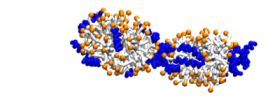	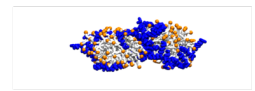
View 3	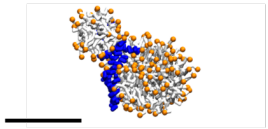	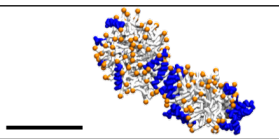	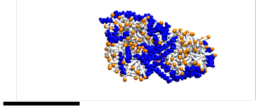

Figure 17. Structural differences regarding the mole ratio of r4F peptide to DMPC

3.3 Conclusion

We implemented direct comparison between eHNP-A1 and eHNP-r4F to explore the structural role of membrane protein and peptides in HDL form. Microfluidic synthesis platform successfully provided both eHNP-A1 and eHNP-r4F nanoparticles which have

similar morphology in shape, size, and composition. The only difference was nanoparticle's stability that particle aggregation has been observed in eHNP-r4F after 7 days from particle synthesis. MD simulation has been performed to demonstrate the stability of nanoparticles by showing structural differences. Simulation results have shown distinct differences of the structure between eHNP-A1 and eHNP-r4F. While apoA1 completely encompassed DMPC bilayer forming eHNP-A1, r4F peptides did not encircle DMPC bilayer, aggregating each other. This led the exposure of hydrophobic tail of DMPC, in water, and this caused nanoparticle aggregation. Increasing the ratio of r4F to DMPC may help r4F peptides to rise the chance to cover hydrophobic region of lipid, avoiding lipid molecule aggregation.

3.4 Methods

3.4.1 MD simulation

The MD simulations were performed using the GROMACS software package [70]. The coarse-grained model for the simulations was done with the MARTINI coarse grain force field [56] for biomolecular systems. Combining the ElneDyn elastic network model [57] with the coarse grain molecular force field to maintain the secondary and tertiary structure of apoA1, we simulated the self-assembly of eHNP-A1 in a 15 x 15 x 15 nm simulation box with a periodic boundary and a trajectory of 1000 ns. The initial conditions of the simulation involved 2 apoA1 molecules arranged in antiparallel around 160 DMPC lipids using the *insane* method for lipid bilayers. Using the same boundary box size of 15 x 15 x 15 nm and number of lipids, we initiated 1 μs trajectory eHNP-r4F simulations with

varying protein: lipid molecular ratios based on our eHNP-A1 simulations and on past simulations using the apoA1-mimetic peptides 18A and 4F [80]. To examine the aggregation of multiple eHNP-r4F particles, we used the initial conditions of a 30 x 30 x 30 nm simulation box and a protein: lipid molecular ratio of 1:16 for a trajectory of 3.5 μs.

3.4.2 eHNP synthesis and characterization

The synthesis conditions used for all NPs were with a Reynolds number of 50, where the flow ratio between the side streams and the center stream was 5.5:1 respectively. The NP precursor solutions included a lipid solution that was composed of DMPC with a concentration of 2.75 mg/mL in 200 proof ethanol, and a protein solution that had either apoA1 or r4F with a concentration of 0.2 mg/mL in PBS (1X, pH 7.4). Syringe pumps from Harvard Apparatus (Holliston, MA) were used to pump the solutions into the device, from which the mixed solution was collected and then triple washed with PBS using a 10,000 M.W. (30,000 M.W. when incorporating DOX or fluorescent labels) centrifugal filter from EMD Millipore Corporation (Darmstadt, Germany) at a speed of 3900 rpm for 20 minutes. The size distribution of the final washed sample was measured with a Zetasizer Nano ZS from Malvern Instruments (Worcestershire, United Kingdom). Protein and lipid precursor compositions between eHNP-A1 and eHNP-r4F were tuned to achieve an average size of 10 nm.

3.5 Supporting information

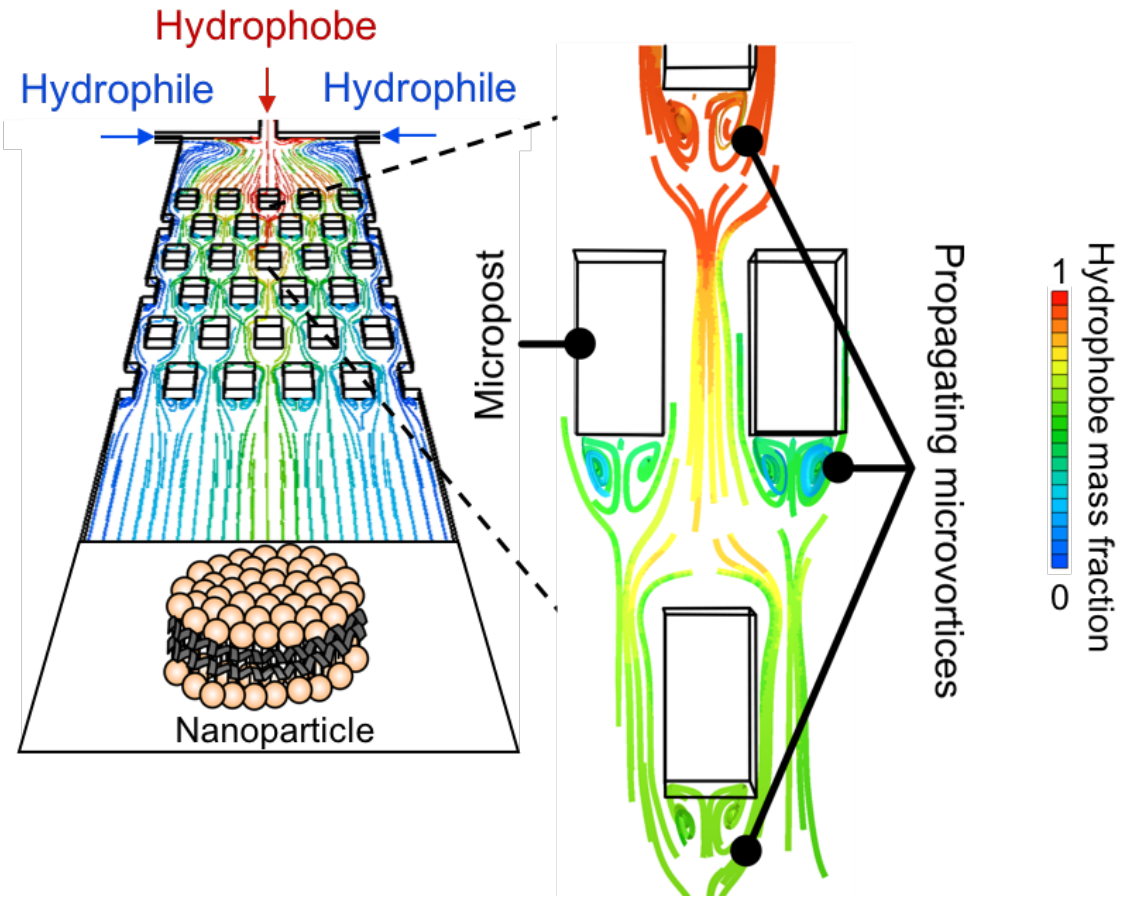

Figure S 1. Microvortex propagation mixer for high throughput nanoparticle synthesis with micropost in the channel

CHAPTER 4. PREDICTION OF PARAOXONASE-1 BINDING STRUCTURE AND MECHANISM AGAINST EHNP-A1

4.1 Background

4.1.1 Paraoxonase-1 as HDL-associated proteins

As it has been explained that HDL components are dynamically modified during complex biological processes, inducing a heterogeneous feature of HDL and causing altered endothelial effects of HDL. For example, paraoxonase-1 (PON1), one of enzymes of HDL, contributes to the atheroprotective function of HDL [28, 81, 82], whereas HDL-bound serum amyloid A (SAA) becomes pro-inflammatory [32]. Due to the overwhelming number of HDL components, however, the mechanisms of the altered effects remain poorly understood [36, 37].

4.1.2 Roles of PON1 with HDL

As mentioned, PON1 is a major anti-atherogenic related protein with HDL. Several studies have shown protective roles against atherosclerosis both *in vitro* and *in vivo*. In terms that lipid oxidation is major cause of atherosclerosis, there have been many experimental evidences that PON1 prevents LDL oxidation in vitro [61, 83, 84], as well as PON1 level has inverse association with the risk for CVD [85].

4.1.3 PON1 structure

PON1 has 354 amino acids and the weight of PON1 is 43kDa. It has two major alpha helices (H1 and H2), which are known as anchoring site when interacting with HDL, because of its hydrophobicity [86]. Although the structure of PON1 has been extensively studied, it is still unclear about how the PON1 binds to HDL, which is critical to demonstrate the function of HDL.

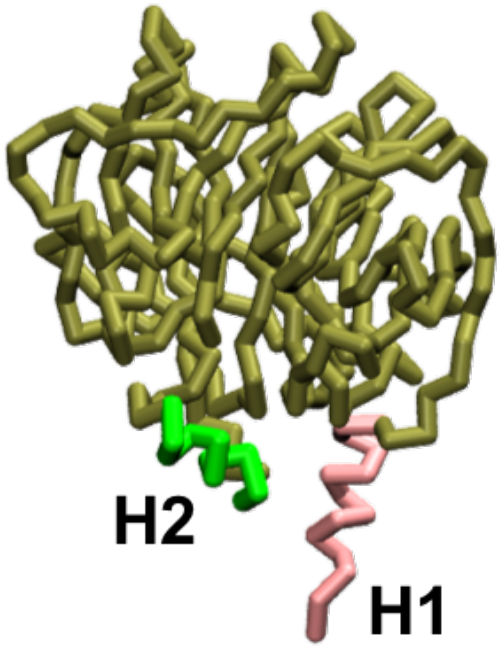

Figure 18. Paraoxonase-1 structure for coarse-grained model

4.1.4 Expected PON1 binding structure to HDL

Knowing binding structure is critical to demonstrate potential binding mechanism, which allow us to expect the function of molecules. Fortunately, PON1 structure is well

documented to implement MD simulation. Before the implementation of simulations to find preferable PON1 binding structure to HDL, I predicted final PON1 binding structure based on literature studies. This is an essential step to reduce simulation time significantly by setting up proper initial configuration. Theoretically proposed model has demonstrated the reason why two major alpha helices of PON1 were involved in interaction with HDL, and several studies have shown PON1 and apoA1 interaction (protein-protein interaction).

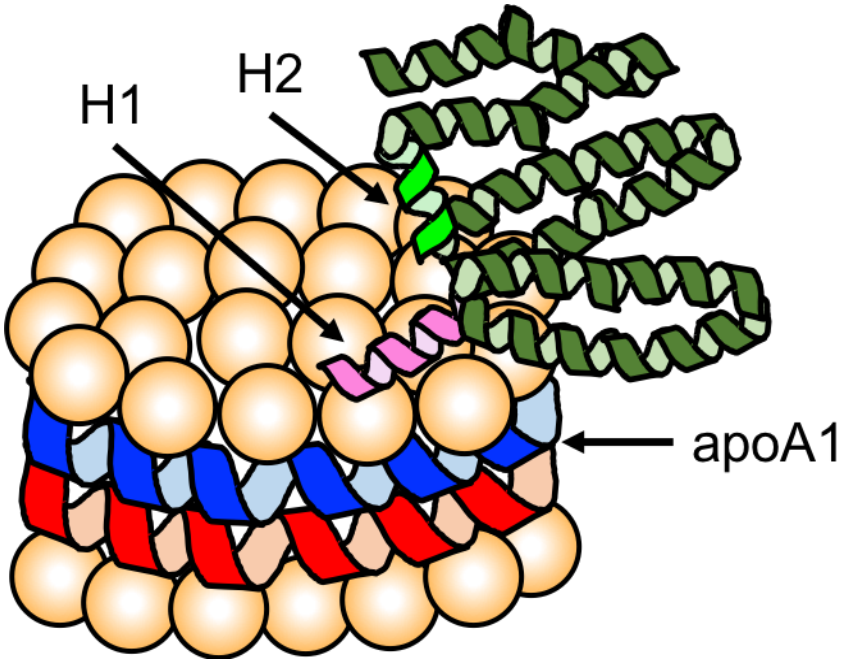

Figure 19. Conceptual model of PON1 binding to eHNP-A1

Based on this background, I expected PON1 binding structure to HDL that two alpha helices of PON1 directed towards the hydrophobic core, and PON1 would be found in the marginal region of apoA1.

4.2 Results

4.2.1 Preferable PON1 binding structure to eHNP-A1

we proved the interaction of PON1 with the aforementioned -A1 model with 1:80 of apoA1-to-DMPC ratio, which was the most relevant ratio for our eHNP-A1 from the microfluidic synthesis. 6 different CG MD simulations were performed to explore preferable binding structure to eHNP-A1. To judge binding stability and binding strength, RMSD and interaction energy were calculated, respectively.

4.2.1.1 6 Initial configurations for parametric study

Prediction of accurate protein binding is still difficult in this field, because energy landscape is generally complicated with many local minima. In other words, protein may easily interact to particular site of molecule, where the local minima exist. For this reason, so many simulations have to be planned to find global minima, statistically. In this work, I conducted 6 MD simulations, placing PON1 molecule in 6 different locations against eHNP-A1. Besides two major alpha helices of PON1 faced towards the hydrophobic core of eHNP-A1.

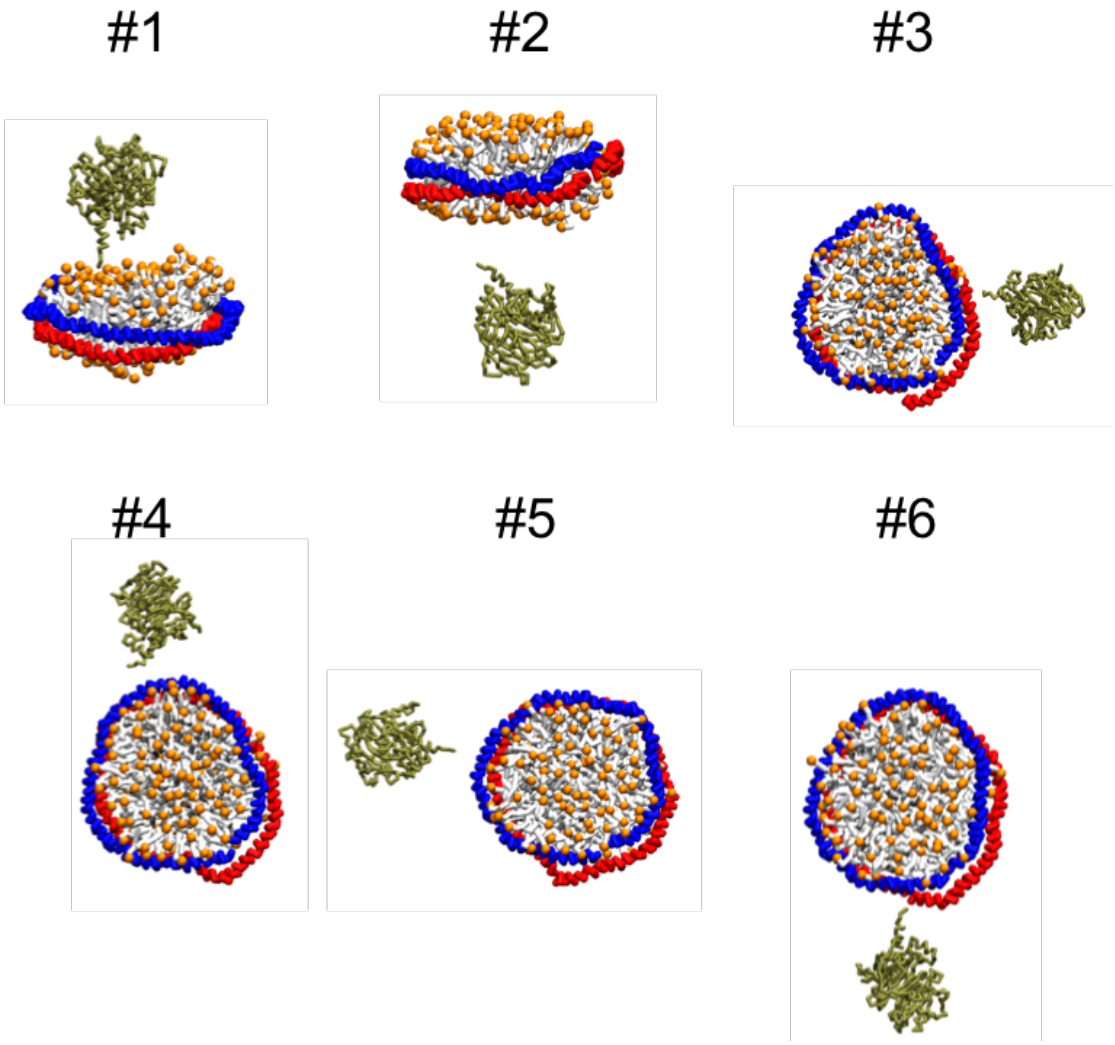

Figure 20. 6 initial configurations to find preferable PON1 binding structure to eHNP-A1

4.2.1.2 Hydrophobic interaction of final binding structures

All simulations have run through 1000 ns, which were enough time to say convergence. In final structures, each PON1 were located at the outer of apoA1-ring, although detailed configurations were different. And the binding was mainly driven by hydrophobic interaction (LJ potential dominant). Interestingly, the three configurations (#1, 5, 6) look similar in terms that two alpha helices of PON1 faced towards the hydrophobic core of eHNP-A1. And those three binding structures are agreed with expected model based on

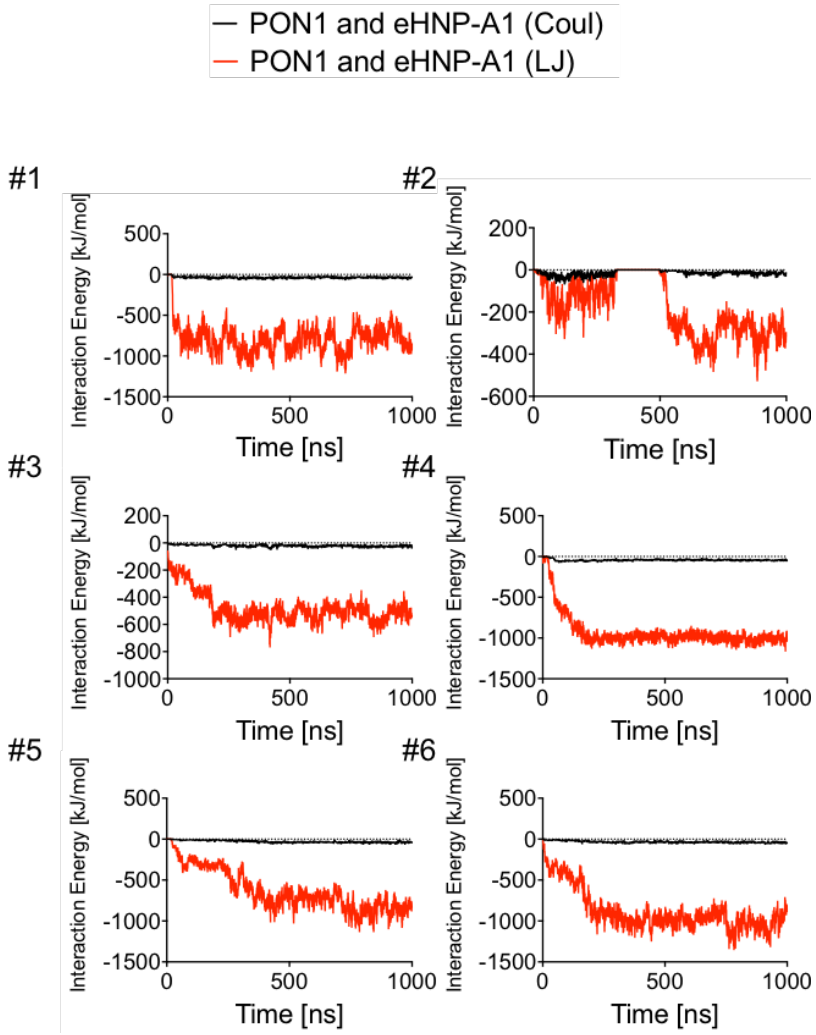

Figure 21. Hydrophobic binding mechanism of eHNP-A1-PON1

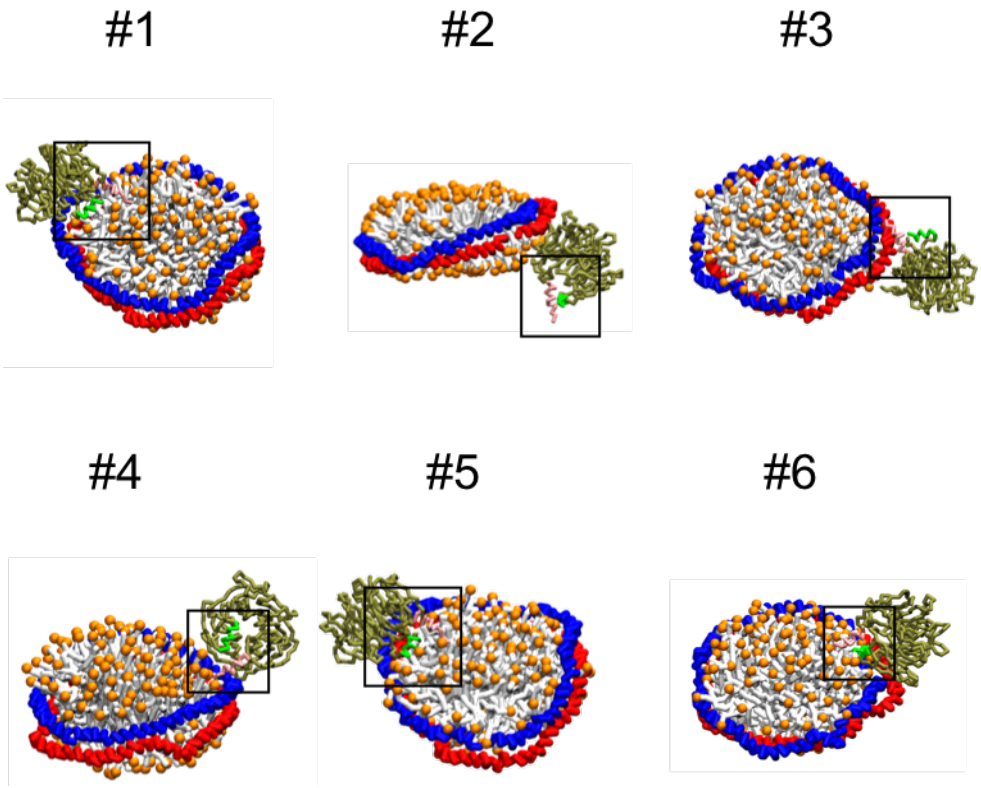

Figure 22. Final binding structures

theoretical proposal. So, it would be good to analyze binding strength and molecule stability to confirm preferable PON1 binding structure to eHNP-A1.

4.2.1.3 Interaction energy analysis between PON1 and eHNP-A1

Four configurations (#1, 4, 5, 6) yielded relatively high attractive interaction of PON1 to eHNP-A1, whereas configuration #2 and 3 exhibited low attraction. In detailed analysis of high attractive cases, configuration #1, 5, 6 showed that the location of H1 and H2 was obviously headed to the hydrophobic core of nanoparticle, while the PON1 was located

near the marginal region of eHNP-A1, suggesting the interaction of PON1 and apoA1 as well.

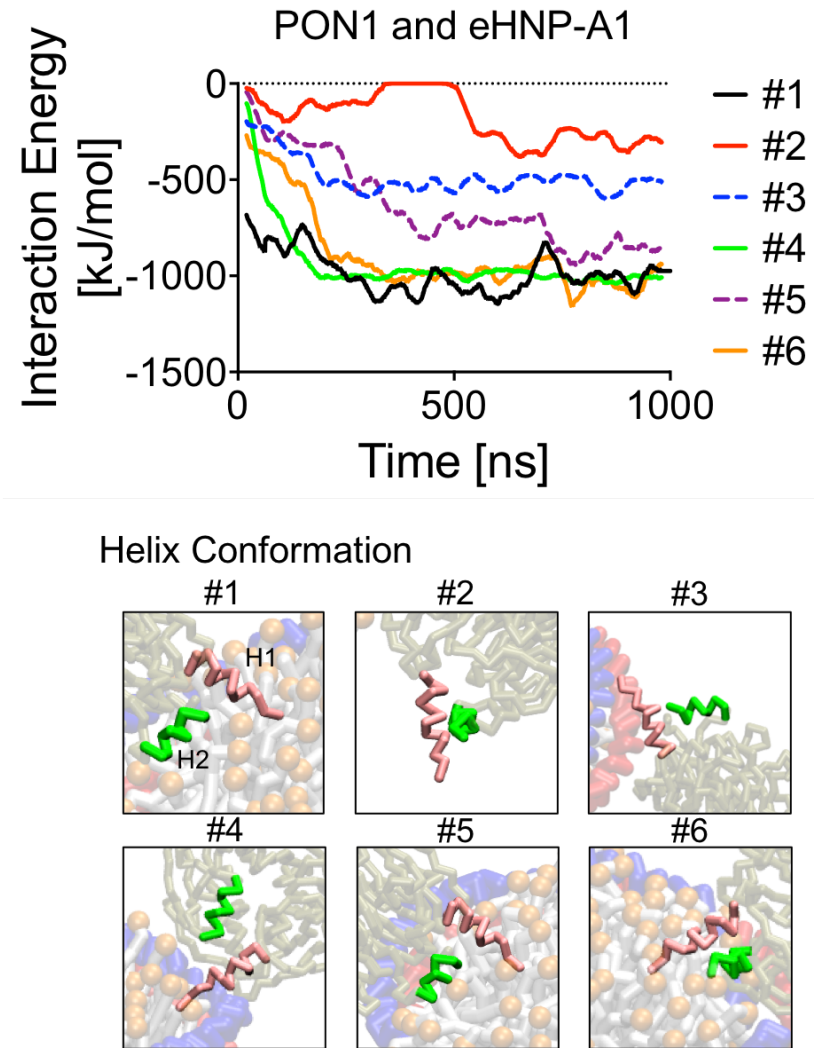

Figure 23. Interaction energy analysis for PON1 binding strength to eHNP-A1

4.2.1.4 Interaction energy analysis between PON1 and apoA1

Interestingly, configuration #4, which also showed strong interaction energy, showed that PON1 interacted mainly with apoA1, while H1/H2 were not oriented toward the core of nanoparticle, implying relatively weak contribution of H1 and H2 to the binding. Besides, apoA1 dominant interaction increased degree of freedom of PON1 that gave a chance to rise mobility.

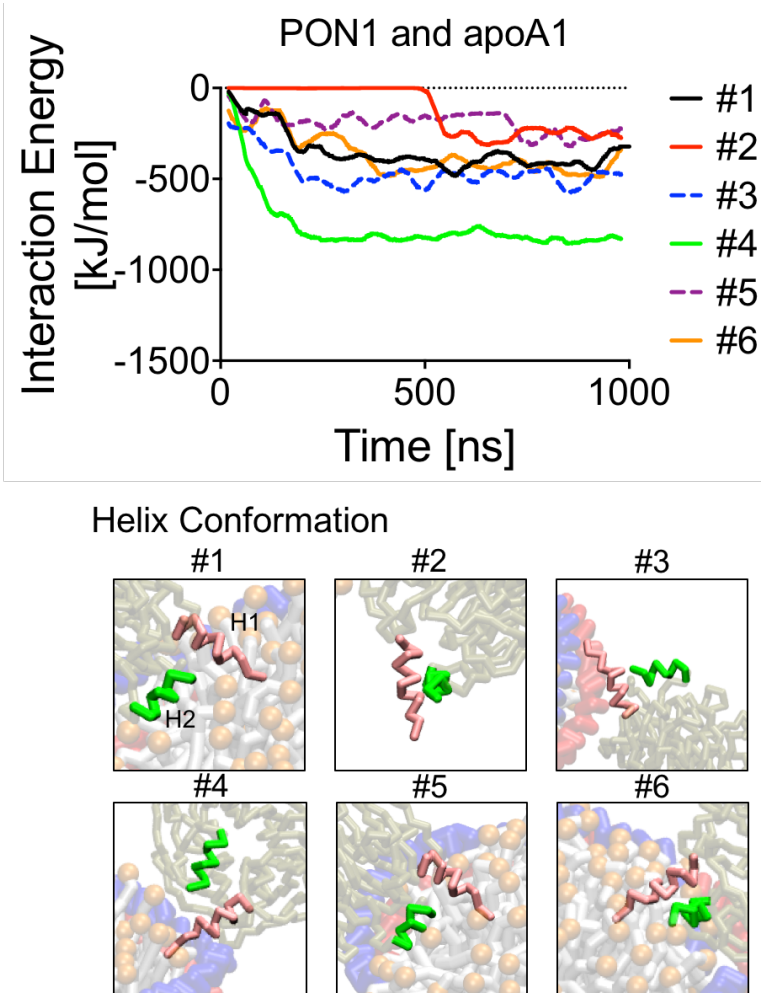

Figure 24. Interaction energy analysis for PON1 binding strength to apoA1

4.2.1.5 Binding stability of PON1

As a next, I analyzed the root mean square deviation (RMSD) of PON1 on eHNP-A1 to demonstrate the structural stability of the PON1 binding. Although configuration #4 exhibited high binding attraction, it exhibited the highest RMSD value, meaning the structural instability of eHNP-A1-PON1 in this configuration. This result is closely connected to the results from the interaction energy between PON1 and apoA1 in eHNP-

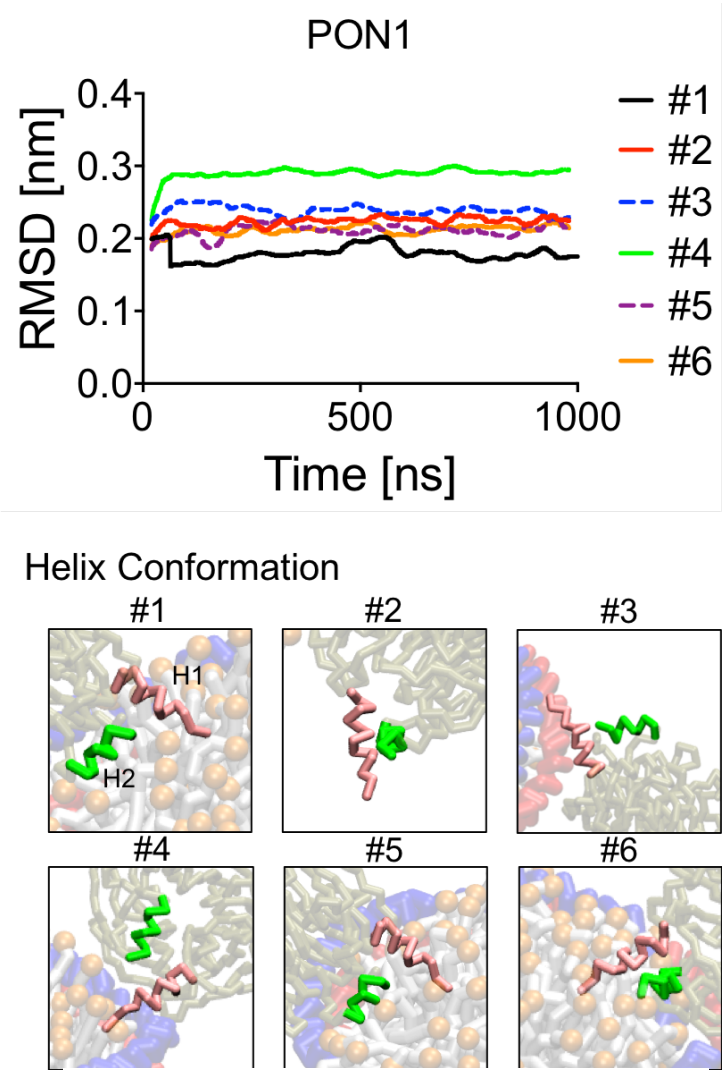

Figure 25. RMSD comparison for structural stability

A1. Interaction energy analysis showed dominant interaction strength between PON1 and apoA1 in #4, and this increased degree of freedom of PON1 that led to lose binding stability.

4.2.1.6 Preferable PON1 binding structure to eHNP-A1

Therefore, we suggest a preferable binding structure of eHNP-A1-PON1 based on our computational analyses; PON1 is located outer ring of eHNP-A1 near apoA1 with two major alpha helices of PON1 directed toward the hydrophobic core of eHNP-A1. This preferable binding structure is also agreed with the theoretically proposed model and experimental results.

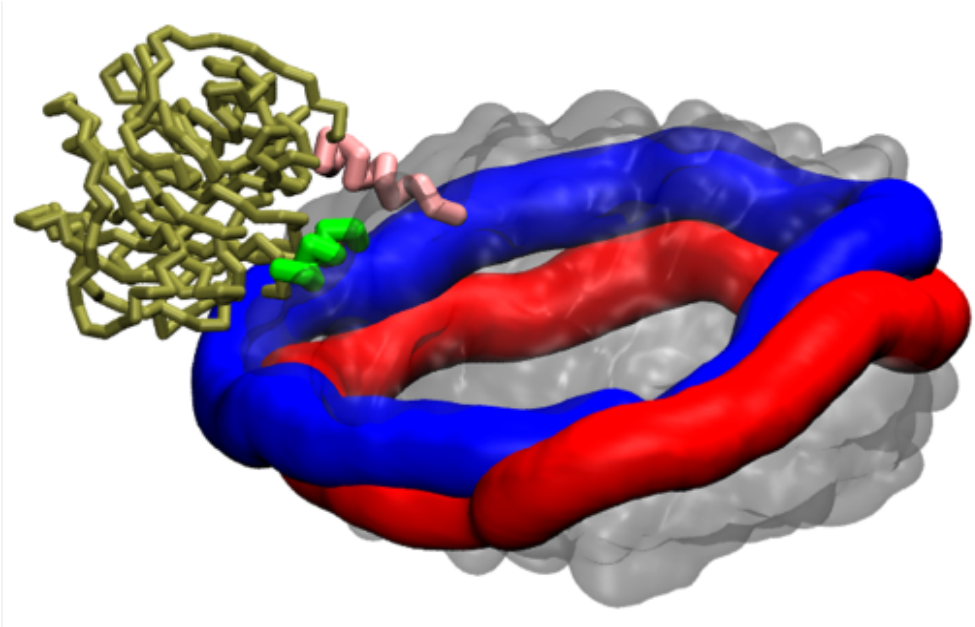

Figure 26. Preferable PON1 binding structure to eHNP-A1

4.2.2 eHNP-A1-PON1 model with experimental correlation

In the final PON1 binding structure on eHNP-A1 (eHNP-A1-PON1), PON1 was found near the outer ring of HDL-A1, where double belted two apoA1s are located. In detail, two major alpha helices of PON1 were towards the hydrophobic lipid core of eHNP-A1 by anchoring on DMPC, while the other parts of PON1 bound to apoA1, suggesting the combinatorial interaction of alpha helices of PON1 with lipid core and protein-protein interaction of PON1 and apoA1. The binding of PON1 on HDL-A1 did not alter the original dimension formed by DMPC and apoA1, but the marginal location of PON1 contributed slight size increase. We then investigated the correlation between modelled eHNP-A1-PON1 and experimentally synthesized eHNP-A1-PON1. By comparing to the morphology and size of eHNP-A1, PON1 in eHNP-A1-PON1 was found on the side of eHNP-A1, where apoA1s were located, demonstrating the strong correlation with our simulation results.. Enzymatic activity of PON1 in eHNP-A1-PON1 was significantly higher as expected, due to PON1 activity stabilization by HDL nanoparticles and apoA1[87-90], adding evidences of the successful realization of the binding of PON1 on eHNP-A1 in our synthesis approach.

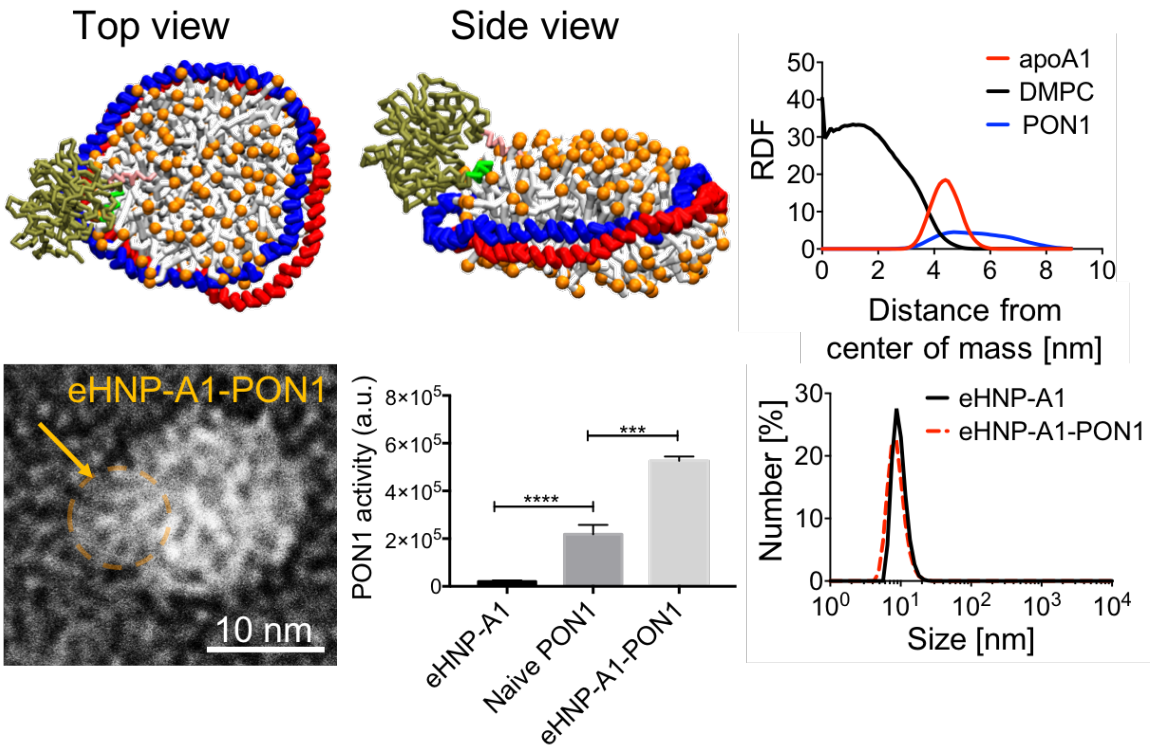

Figure 27. Morphology comparison between eHNP-A1 and eHNP-A1-PON1 with computational and experimental approach. PON1 enzyme activity. ***p < 0.001, ****p < 0.0001

4.2.3 Multiple PON1 binding possibility

Multiple PON1 binding was also observed in both approaches. No one has showed about multiple PON1 binding. MD simulation provided the possibilities that HDL could interact with more than a single PON1. Although we found out the image of two PON1 binding to eHNP-A1 in particular region in a TEM grid, more works are needed to verify and propose its significance. Also, the TEM image might be controversial, questioning that how we can recognize that the two particles are PON1. Not like computational simulation, one

difficulty in experiment is that there is no way to synthesize 2 PON1 with 1 eHNP-A1 on purpose, even though we use 2 to 1 ratio for synthesis.

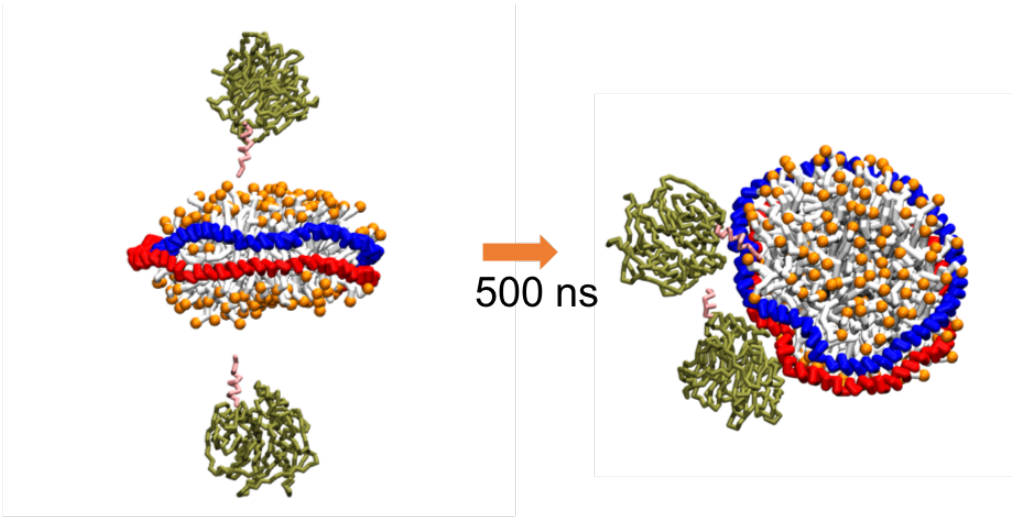

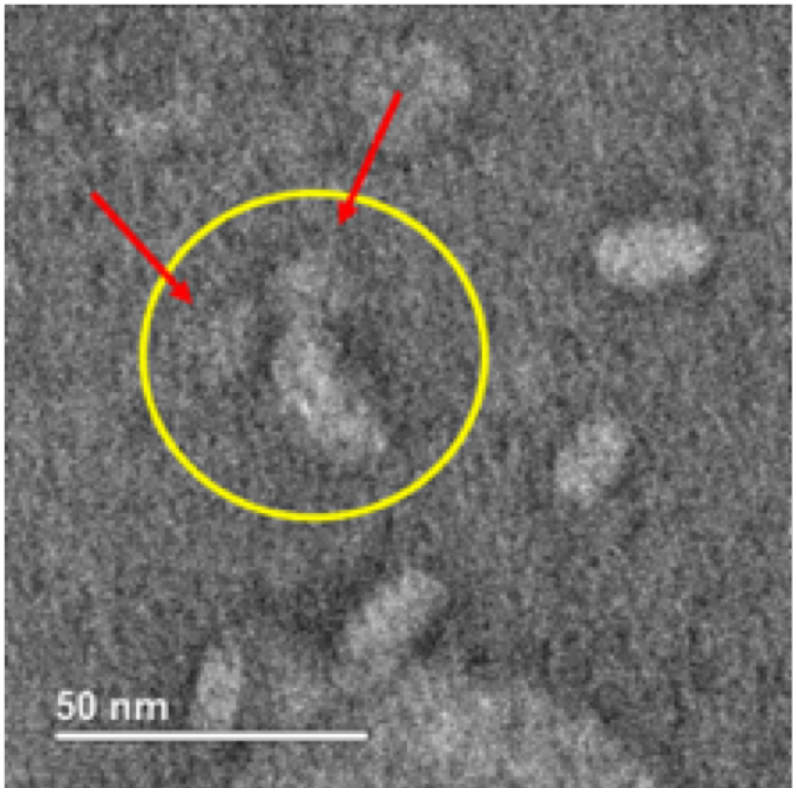

Figure 28.. Multiple PON1 binding to discoidal eHNP-A1

4.2.4 PON1 binding to spherical form of eHNP-A1

HDL particles exist in various forms in the physiological condition, from discoidal to spherical shape [6]. Recent studies have showed the enzymatic activity of PON1 varies with different HDL subclasses [91-93], therefore, it is critical to understand PON1 binding to different compositions and/or shapes of HDL nanoparticles. I further performed PON1 binding to the two spherical eHNP-A1s, double-belt and trefoil to investigate apoA1 structure dependent. Interestingly, PON1 successfully bound to the double-belt eHNP-A1, but not with the trefoil eHNP-A1, suggesting specific apoA1 configuration is critical for the binding of PON1 to eHNP-A1. A series of these results suggests that the conformation of apoA1 in functionally active PON1-HDL might be a double-belted form in the

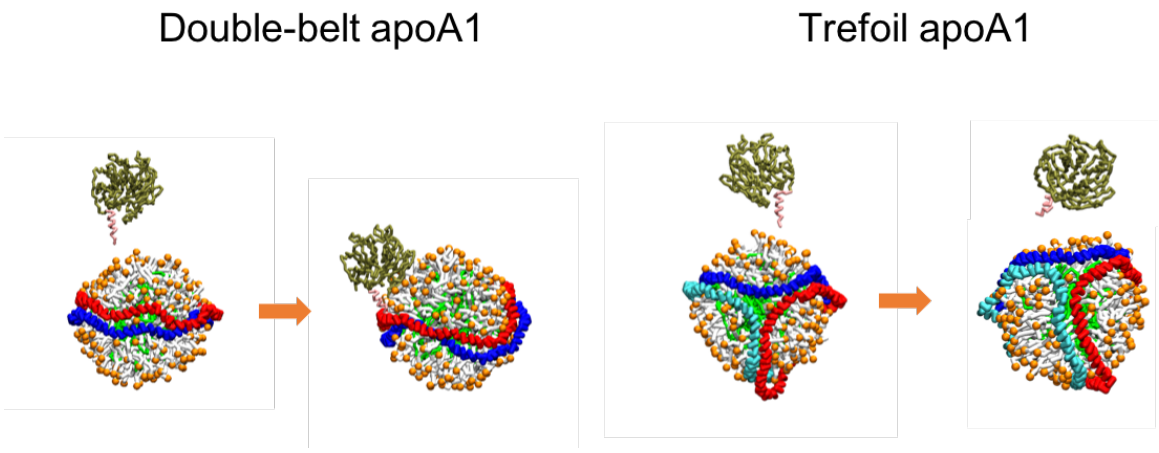

Figure 29. PON1 binding to other forms and composition of eHNP-A1

physiological condition.

4.3 Conclusion

CG MD simulations have been performed to explore one of HDL-associated proteins, PON1 binding to eHNP-A1. It is important to know the protein binding structure in terms

that we can ultimately predict the function of molecule based on that. 6 different PON1 orientations have been implemented to prove preferable PON1 binding structure with interaction energy analysis and binding stability. Comprehensive analysis supported preferable binding structure, and that structure is also agreed with theoretically proposed model and past experiments. Even with the experimental correlation, our proposal of PON1 binding structure to eHNP-A1 was verified. With this computational power, I explored PON1 binding to spherical eHNP-A1 with two different apoA1 structure, which were hard to control the apoA1 structure in HDL in experiment. The results showed that PON1 binding depended on apoA1 structure.

4.4 Discussion

I have explored the binding between PON1 and eHNP-A1, and suggested PON1 binding structure and mechanism to eHNP-A1. Simulation results were closely agreed with theoretical model and our experimental results. As there are various other HDL-associated proteins, my simulation approach would be good to apply for binding mechanism to HDL. And this is critical to predict the function of HDL with HDL-associated proteins, because recent studies have shown dysfunctional HDL regarding which enzyme protein interact with.

4.5 Methods

4.5.1 MD simulation

GROMACS 4.5.7 [70] was used as MD simulation software package with MARTINI force field [56] in conjunction with ElNeDyn[57] to maintain secondary and tertiary structure.

Double-belt apoA1 structure was obtained from CHARMM-GUI [71, 72]. DMPC molecules were used as phospholipid. For 3 simulation cases, 120, 160, and 200 number of DMPC bilayer molecules were located inside of double belt apoA1 in 15 x 15 x 15 x nm sized simulation box, as an initial configuration. The system was solvated with water molecules and neutralized with Na^+ counterions. Then, this system was energy minimized with steepest descent algorithm for 5000 steps. Next, equilibrium step was performed with molecule restraints. Simulation time step, 20 fs was set up, which is proper range in MARTINI force field. Total simulation time, 1000 ns was set for all simulations. Temperature kept 298K for RT.

4.5.2 Synthesis of eHNP-A1 and eHNP-A1-PON1

A three-inlet microfluidic device that generates propagating microvertices was used for a single-step self-assembly of eHNP-A1 according to the previous report with slight modification. In brief, 1,2-dimyristoyl-sn-glycero-3-phosphocholine (DMPC, Avanti Polar Lipids, AL; 2.75 mg/mL) in absolute ethanol was introduced into the center inlet of the microfluidic device at a flow rate of 0.8 mL/min. Apolipoprotein A1 (Millipore Sigma, MA; 0.2 mg/mL) in phosphate buffered saline (PBS, pH = 7.4) was introduced into two outer inlets at a flow rate of 2.2 mL/min. Each of DMPC and apoA1 solution was homogenously injected using a programmable syringe pump (Harvard Apparatus, MA) at the desired flow rates. After running the syringe pump, the mixture solution was collected from outlet, followed by transferring the solution to centrifugal membrane filter (EMD Millipore, Germany) with a molecular weight cut off (MWCO) of 50,000, and purified 5

times in PBS at a speed of 3900 rpm for 30 min. Synthesized eHNP-A1 was stored at 4°C for further modification.

For PON-1 incorporation, medium of eHNP-A1 was replaced from PBS to Hank's Balanced Salt Solution (HBSS, pH = 7.4). After quantification of apoA1 in eHNP-A1 using BCA assay according to the manufacturer's protocol, 0.5 equivalent PON1 to apoA1 was added to eHNP-A1, and incubated for 2 h at 37 °C with gentle pipetting for every 15 min. After the incubation, the solution was transferred to centrifugal membrane filter (EMD Millipore, Germany) with a MWCO of 50,000, and purified 3 times in HBSS at a speed of 3900 rpm for 20 min. The purified solution was stored at 4°C.

4.5.3 Characterization of eHNP-A1 and eHNP-A1-PON1

Hydrodynamic volume of eHNP-A1 and eHNP-A1-PON1 were obtained by a Zetasizer Nano (Malvern Instrument, Malvern, UK). The amount of PON1 in eHNP-A1-PON1 was quantified by running sodium dodecyl sulfate poly(acrylamide) gel electrophoresis (SDS-PAGE, separating phase of 12% acrylamide), and calculating the band intensity using imageJ software. PON1 activity of naïve PON1, eHNP-A1-PON1, and corresponding amout of eHNP-A1 was analyzed by EnzChek paraoxonase assay kit (Thermo Fisher) according to the manufacturer's protocol. For the monitoring of size and morphology of eHNP-A1 and eHNP-A1-PON1, negatively stained samples were observed using a transmission electron microscope (TEM; Hitachi 7700, Hitachi, Japan) at 120kV coupled with the Digital Micrograph camera and software suite from Gatan.

4.6 Supporting information

4.6.1 eHNP-A1 and eHNP-A1-PON1 comparison in TEM and DLS

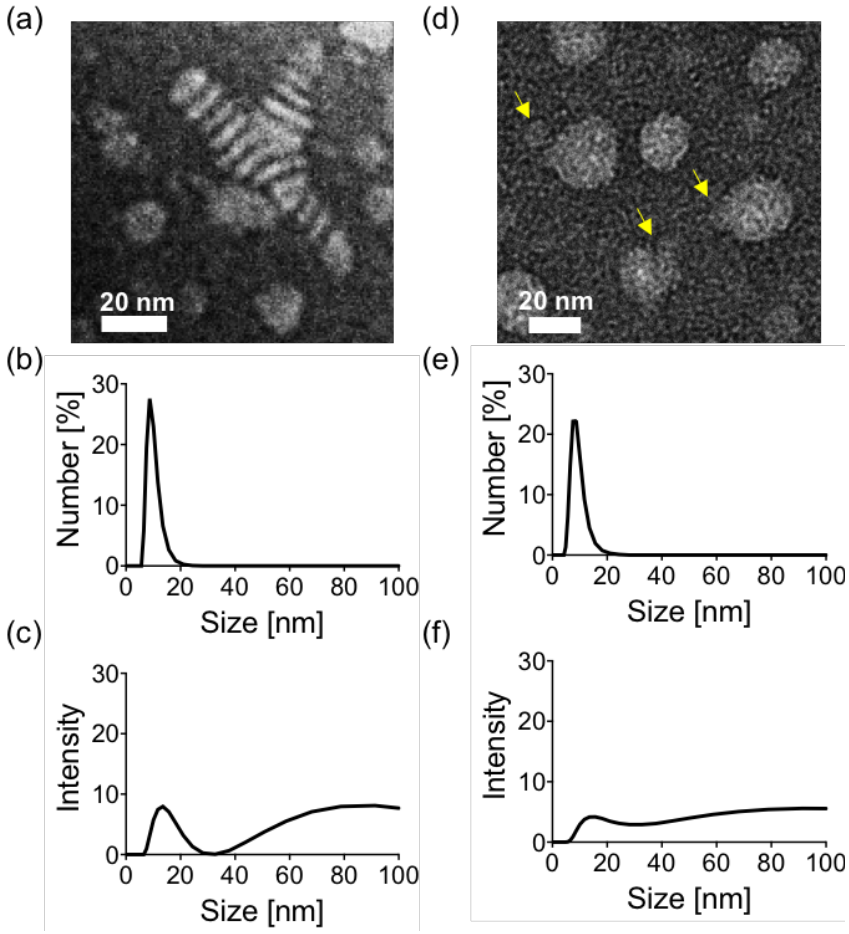

Figure S 2. Figure S1. Morphology of eHNP-A1 and eHNP-A1-PON1 from experiment. (a) TEM image of eHNP-A1 (b) DLS size distribution of eHNP-A1 in number (c) DLS size distribution of eHNP-A1 in intensity (d) TEM image of eHNP-A1-PON1 (e) DLS size distribution of eHNP-A1-PON1 in number (f) DLS size distribution of eHNP-A1-PON1 in intensity

4.6.2 The role of apoA1 in PON1 binding

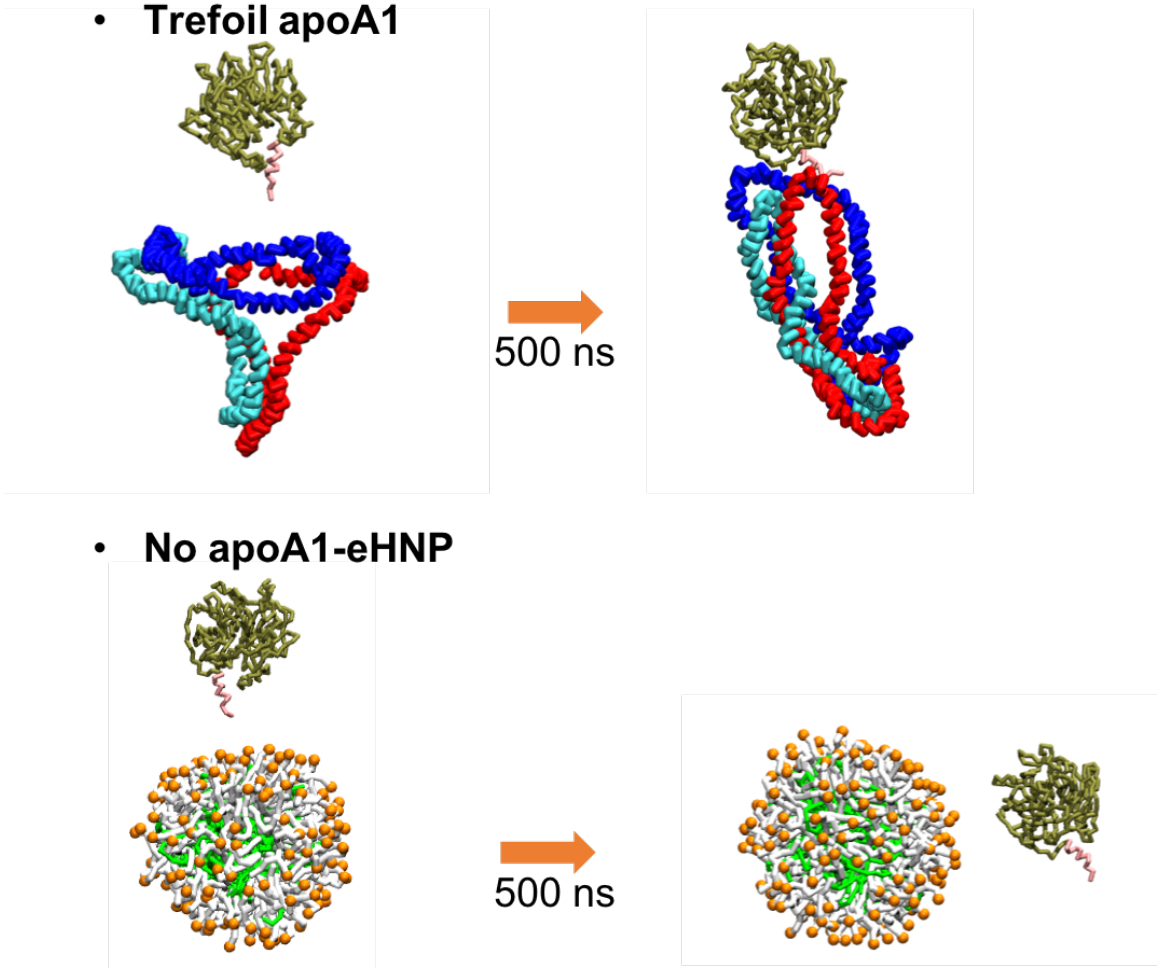

Figure S 3. Simulations of PON1 binding to diverse cases. Top) PON1 binding with trefoil apoA1. Bottom) PON1 binding eHNP-A1 without apoA1

CHAPTER 5. CONCLUSION

HDL has long been studies because of its importance in term of inverse association with cardiovascular disease, which is top cause of death in US. For this reason, HDL research has been comprehensively documented regarding the structure, function, and HDL associated protein enzymes. HDL is a multifunctional nanoparticle, as well as it has various shapes and compositions. However, the heterogeneous popularity is still a major hurdle to investigate the characteristics of HDL nanoparticle.

Despite of heterogeneity of HDL, the various approaches to HDL research has also been suggested because of the importance of HDL. Reconstituted HDL has been developed with major components of HDL as simplified form. And microfluidics technology has been applied to synthesize homogeneous nanoparticles with high reproducibility. Further, MD simulation has been introduced to analyze the structure and to predict the function and molecule binding mechanism, along with the development of computer performance. Although HDL structure, function, and the relation to HDL-associated proteins have been well documented with given approaches, other unexpected function of HDL has been shown in recent clinical studies. In other words, HDL cannot be anymore called “Good cholesterol”. It has been known that dysfunctional HDL is related to HDL-associated proteins. For example, PON1 functionalizes HDL as anti-inflammatory and antioxidative roles. On the other hand, SAA induces pro-inflammatory.

In my work, I applied MD simulation approach to explore HDL-mimetic nanoparticles. MD simulation is one approach that enables molar level analysis that helps to understand nanoparticle structure, function and molecule binding mechanism. With this approach, I was able to investigate HDL-mimetic nanostructures, which has yet to be explored. After validate MD simulation setup with experimental correlations, I have shown that structural

deformation of discoidal eHNP-A1 suggesting maximum loading capacity. Further, structural analysis revealed why apoA1-mimetic peptide-based nanostructure has less stability than apoA1-based nanoparticle with the advantage of MD simulation. Finally, I proposed preferable PON1 binding structure to eHNP-A1, which is important to predict HDL function and binding mechanism.

There are still many things to do with MD simulation regarding HDL research, such as the structural analysis with different compositions and shapes, and the binding structure prediction with other HDL-associated proteins to propose. My approach would definitely help to uncover the areas where have yet to be clear.

REFERENCES

1. Ribeiro, J.V., et al., *QwikMD - Integrative Molecular Dynamics Toolkit for Novices and Experts.* Sci Rep, 2016. **6**: p. 26536.

2. Gordon, D.J., et al., *High-density lipoprotein cholesterol and cardiovascular disease. Four prospective American studies.* Circulation, 1989. **79**(1): p. 8-15.

3. Tall, A.R., *An overview of reverse cholesterol transport.* Eur Heart J, 1998. **19 Suppl A**: p. A31-5.

4. Marques, L.R., et al., *Reverse Cholesterol Transport: Molecular Mechanisms and the Non-medical Approach to Enhance HDL Cholesterol.* Front Physiol, 2018. **9**: p. 526.

5. Lund-Katz, S. and M.C. Phillips, *High density lipoprotein structure-function and role in reverse cholesterol transport.* Subcell Biochem, 2010. **51**: p. 183-227.

6. Kontush, A., et al., *Structure of HDL: particle subclasses and molecular components.* Handb Exp Pharmacol, 2015. **224**: p. 3-51.

7. Barrans, A., et al., *Pre-beta HDL: structure and metabolism.* Biochim Biophys Acta, 1996. **1300**(2): p. 73-85.

8. Phillips, M.C., *New insights into the determination of HDL structure by apolipoproteins: Thematic review series: high density lipoprotein structure, function, and metabolism.* J Lipid Res, 2013. **54**(8): p. 2034-48.

9. Bibow, S., et al., *Solution structure of discoidal high-density lipoprotein particles with a shortened apolipoprotein A-I.* Nat Struct Mol Biol, 2017. **24**(2): p. 187-193.

10. Yvan-Charvet, L., N. Wang, and A.R. Tall, *Role of HDL, ABCA1, and ABCG1 transporters in cholesterol efflux and immune responses.* Arterioscler Thromb Vasc Biol, 2010. **30**(2): p. 139-43.

11. Oram, J.F., *HDL apolipoproteins and ABCA1: partners in the removal of excess cellular cholesterol.* Arterioscler Thromb Vasc Biol, 2003. **23**(5): p. 720-7.

12. Duong, P.T., et al., *Characterization of nascent HDL particles and microparticles formed by ABCA1-mediated efflux of cellular lipids to apoA-I.* J Lipid Res, 2006. **47**(4): p. 832-43.

13. Segrest, J.P., S.C. Harvey, and V. Zannis, *Detailed molecular model of apolipoprotein A-I on the surface of high-density lipoproteins and its functional implications.* Trends Cardiovasc Med, 2000. **10**(6): p. 246-52.

14. Li, L., et al., *Double belt structure of discoidal high density lipoproteins: molecular basis for size heterogeneity.* J Mol Biol, 2004. **343**(5): p. 1293-311.

15. Thomas, M.J., S. Bhat, and M.G. Sorci-Thomas, *Three-dimensional models of HDL apoA-I: implications for its assembly and function.* J Lipid Res, 2008. **49**(9): p. 1875-83.

16. Rousset, X., et al., *Lecithin: cholesterol acyltransferase--from biochemistry to role in cardiovascular disease.* Curr Opin Endocrinol Diabetes Obes, 2009. **16**(2): p. 163-71.

17. Haase, C.L., et al., *LCAT, HDL cholesterol and ischemic cardiovascular disease: a Mendelian randomization study of HDL cholesterol in 54,500 individuals.* J Clin Endocrinol Metab, 2012. **97**(2): p. E248-56.

18. Barter, P.J., *Hugh sinclair lecture: the regulation and remodelling of HDL by plasma factors.* Atheroscler Suppl, 2002. **3**(4): p. 39-47.

19. de la Llera-Moya, M., et al., *Scavenger receptor BI (SR-BI) mediates free cholesterol flux independently of HDL tethering to the cell surface.* J Lipid Res, 1999. **40**(3): p. 575-80.

20. Acton, S., et al., *Identification of scavenger receptor SR-BI as a high density lipoprotein receptor.* Science, 1996. **271**(5248): p. 518-520.

21. Nieland, T.J., et al., *Discovery of chemical inhibitors of the selective transfer of lipids mediated by the HDL receptor SR-BI.* Proc Natl Acad Sci U S A, 2002. **99**(24): p. 15422-7.

22. Gursky, O., *Structural stability and functional remodeling of high-density lipoproteins.* FEBS Letters, 2015. **589**(19PartA): p. 2627-2639.

23. Mulder, W.J.M., et al., *High-Density Lipoprotein Nanobiologics for Precision Medicine.* Acc Chem Res, 2018. **51**(1): p. 127-137.

24. Roger S. Newton, B.R.K., *HDL therapy for the accute treatment of atherosclerosis.* Atherosclerosis Supplements, 2002. **3**: p. 31-38.

25. Hegele, R.A., *A Glimpse at HDL-based therapy for atherosclerosis.* Clinical Biochemical review, 2004. **25**.

26. Kingwell, B.A., et al., *HDL-targeted therapies: progress, failures and future.* Nat Rev Drug Discov, 2014. **13**(6): p. 445-64.

27. Khera, A.V., et al., *Cholesterol efflux capacity, high-density lipoprotein function, and atherosclerosis.* N Engl J Med, 2011. **364**(2): p. 127-35.

28. Eren, E., N. Yilmaz, and O. Aydin, *Functionally Defective High-Density Lipoprotein and Paraoxonase: A Couple for Endothelial Dysfunction in Atherosclerosis.* Cholesterol, 2013.

29. James, R.W. and S.P. Deakin, *The contribution of high density lipoprotein apolipoproteins and derivatives to serum paraoxonase-1 activity and function.* Adv Exp Med Biol, 2010. **660**: p. 173-81.

30. Pasqualini, L., et al., *Paraoxonase-1 activity modulates endothelial function in patients with peripheral arterial disease.* Atherosclerosis, 2005. **183**(2): p. 349-54.

31. Bhattacharyya, T., et al., *Relationship of paraoxonase 1 (PON1) gene polymorphisms and functional activity with systemic oxidative stress and cardiovascular risk.* JAMA, 2008. **299**(11): p. 1265-76.

32. Han, C.Y., et al., *Serum amyloid A impairs the antiinflammatory properties of HDL.* J Clin invest, 2016. **126**(1): p. 266-281.

33. Kisilevsky, R. and L. Subrahmanyan, *Serum amyloid A changes high density lipoprotein's cellular affinity. A clue to serum amyloid A's principal function.* Lab Invest, 1992. **66**(6): p. 778-85.

34. Banka, C.L., et al., *Serum amyloid A (SAA): influence on HDL-mediated cellular cholesterol efflux.* J Lipid Res, 1995. **36**(5): p. 1058-65.

35. Weichhart, T., et al., *Serum amyloid A in uremic HDL promotes inflammation.* J Am Soc Nephrol, 2012. **23**(5): p. 934-47.

36. Besler, C., T.F. Luscher, and U. Landmesser, *Molecular mechanisms of vascular effects of High-density lipoprotein: alterations in cardiovascular disease.* EMBO Mol Med, 2012. **4**(4): p. 251-68.

37. Speer, T., et al., *Abnormal high-density lipoprotein induces endothelial dysfunction via activation of Toll-like receptor-2.* Immunity, 2013. **38**(4): p. 754-68.

38. Jonas, A., Kezdy, K. E., and Wald, J.H., *Defined Apolipoprotein A-I Conformations in Reconstituted High Densith Lipoprotein Discs.* The Journal of Biological Chemistry, 1989. **264**(9): p. 4818-4824.

39. Jonas, A., *Reconstitution of high-density lipoproteins.* Methods Enzymol, 1986. **128**: p. 553-82.

40. Frias, M.A., et al., *Native and reconstituted HDL protect cardiomyocytes from doxorubicin-induced apoptosis.* Cardiovasc Res, 2010. **85**(1): p. 118-26.

41. Cho, K.H., *Synthesis of reconstituted high density lipoprotein (rHDL) containing apoA-I and apoC-III: the functional role of apoC-III in rHDL.* Mol Cells, 2009. **27**(3): p. 291-7.

42. Kim, Y., et al., *Single step reconstitution of multifunctional high-density lipoprotein-derived nanomaterials using microfluidics.* ACS Nano, 2013. **7**(11): p. 9975-83.

43. Ahn, J., et al., *Microfluidics in nanoparticle drug delivery; From synthesis to pre-clinical screening.* Advanced Drug Delivery Reviews, 2018. **128**: p. 29-53.

44. Sei, Y.J., et al., *Detecting the functional complexities between high-density lipoprotein mimetics.* Biomaterials, 2018. **170**: p. 58-69.

45. Jonas, A., et al., *Apolipoprotein A-I structure and lipid properties in homogeneous, reconstituted spherical and discoidal high density lipoproteins.* J Biol Chem, 1990. **265**(36): p. 22123-9.

46. Borhani, D.W., et al., *Crystal structure of truncated human apolipoprotein A-I suggests a lipid-bound conformation.* Proc Natl Acad Sci U S A, 1997. **94**(23): p. 12291-6.

47. Klon, A.E., et al., *Molecular belt models for the apolipoprotein A-I Paris and Milano mutations.* Biophys J, 2000. **79**(3): p. 1679-85.

48. Silva, R.A., et al., *Structure of apolipoprotein A-I in spherical high density lipoproteins of different sizes.* Proc Natl Acad Sci U S A, 2008. **105**(34): p. 12176-81.

49. Hansson, T., C. Oostenbrink, and W.F. van Gunsteren, *Molecular dynamics simulations.* Current Opinion in Structural Biology, 2002. **12**(2): p. 190-196.

50. Klon, A.E., J.P. Segrest, and S.C. Harvey, *Molecular Dynamics Simulations on Discoidal HDL Particles Suggest a Mechanism for Rotation in the Apo A-I Belt Model.* Journal of Molecular Biology, 2002. **324**(4): p. 703-721.

51. Shih, A.Y., et al., *Molecular dynamics simulations of discoidal bilayers assembled from truncated human lipoproteins.* Biophys J, 2005. **88**(1): p. 548-56.

52. Catte, A., et al., *Novel changes in discoidal high density lipoprotein morphology: a molecular dynamics study.* Biophys J, 2006. **90**(12): p. 4345-60.

53. Shih, A.Y., et al., *Coarse grained protein-lipid model with application to lipoprotein particles.* J Phys Chem B, 2006. **110**(8): p. 3674-84.

54. Shih, A.Y., et al., *Assembly of lipoprotein particles revealed by coarse-grained molecular dynamics simulations.* J Struct Biol, 2007. **157**(3): p. 579-92.

55. Shih, A.Y., S.G. Sligar, and K. Schulten, *Molecular models need to be tested: the case of a solar flares discoidal HDL model.* Biophys J, 2008. **94**(12): p. L87-9.

56. Marrink, S.J., et al., *The MARTINI force field: coarse grained model for biomolecular simulations.* J Phys Chem B, 2007. **111**(27): p. 7812-24.

57. Periole, X., et al., *Combining an Elastic Network With a Coarse-Grained Molecular Force Field: Structure, Dynamics, and Intermolecular Recognition.* J Chem Theory Comput, 2009. **5**(9): p. 2531-43.

58. Shih, A.Y., S.G. Sligar, and K. Schulten, *Maturation of high-density lipoproteins.* J R Soc Interface, 2009. **6**(39): p. 863-71.

59. Shih, A.Y., et al., *Disassembly of nanodiscs with cholate.* Nano Lett, 2007. **7**(6): p. 1692-6.

60. Segrest, J.P., et al., *Surface Density-Induced Pleating of a Lipid Monolayer Drives Nascent High-Density Lipoprotein Assembly.* Structure, 2015. **23**(7): p. 1214-26.

61. Mackness, M.I., et al., *Serum paraoxonase activity in familial hypercholesterolaemia and insulin-dependent diabetes mellitus.* Atherosclerosis, 1991. **86**(2-3): p. 193-9.

62. Aviram, M. and M. Rosenblat, *Paraoxonases 1, 2, and 3, oxidative stress, and macrophage foam cell formation during atherosclerosis development.* Free Radical Biology and Medicine, 2004. **37**(9): p. 1304-1316.

63. Karp, G., *Cell and Molecular Biology.* John Wiley & Sons, Inc., 2002.

64. Denisov, I.G., et al., *Directed self-assembly of monodisperse phospholipid bilayer Nanodiscs with controlled size.* J Am Chem Soc, 2004. **126**(11): p. 3477-87.

65. Bayburt, T.H., Y.V. Grinkova, and S.G. Sligar, *Self-assembly of discoidal phospholipid bilayer nanoparticles with membrane scaffold proteins.* Nano Letters, 2002. **2**(8): p. 853-856.

66. Wu, Z., et al., *The low resolution structure of ApoA1 in spherical high density lipoprotein revealed by small angle neutron scattering.* J Biol Chem, 2011. **286**(14): p. 12495-508.

67. Huang, R., et al., *Apolipoprotein A-I structural organization in high-density lipoproteins isolated from human plasma.* Nat Struct Mol Biol, 2011. **18**(4): p. 416-22.

68. Bruce, C., et al., *Molecular determinants of plasma cholesteryl ester transfer protein binding to high density lipoproteins.* J Biol Chem, 1995. **270**(19): p. 11532-42.

69. Siuda, I. and D.P. Tieleman, *Molecular models of nanodiscs.* J Chem Theory Comput, 2015. **11**(10): p. 4923-32.

70. M.J. Abraham, D.v.d.S., E. Lindahl, B. Hess, and the GROMACS development team,, *GROMACS User Manual.* 2019.

71. Jo, S., et al., *CHARMM-GUI: a web-based graphical user interface for CHARMM.* J Comput Chem, 2008. **29**(11): p. 1859-65.

72. Qi, Y., et al., *CHARMM-GUI Nanodisc Builder for modeling and simulation of various nanodisc systems.* J Comput Chem, 2019. **40**(7): p. 893-899.

73. Navab, M., et al., *Human apolipoprotein AI mimetic peptides for the treatment of atherosclerosis.* Curr Opin Investig Drugs, 2003. **4**(9): p. 1100-4.

74. Marrache, S. and S. Dhar, *Biodegradable synthetic high-density lipoprotein nanoparticles for atherosclerosis.* Proceedings of the National Academy of Sciences of the United States of America, 2013. **110**(23): p. 9445-9450.

75. Leman, L.J., B.E. Maryanoff, and M.R. Ghadiri, *Molecules That Mimic Apolipoprotein A-I: Potential Agents for Treating Atherosclerosis.* Journal of Medicinal Chemistry, 2014. **57**(6): p. 2169-2196.

76. Qin, S., et al., *Reverse D4F, an apolipoprotein-AI mimetic peptide, inhibits atherosclerosis in ApoE-null mice.* J Cardiovasc Pharmacol Ther, 2012. **17**(3): p. 334-43.

77. Zhang, Z., et al., *HDL-mimicking peptide-lipid nanoparticles with improved tumor targeting.* Small, 2010. **6**(3): p. 430-7.

78. Cui, L., et al., *A PEGylation-Free Biomimetic Porphyrin Nanoplatform for Personalized Cancer Theranostics.* ACS Nano, 2015. **9**(4): p. 4484-95.

79. Zhang, Z., et al., *Biomimetic nanocarrier for direct cytosolic drug delivery.* Angew Chem Int Ed Engl, 2009. **48**(48): p. 9171-5.

80. Midtgaard, S.R., et al., *Self-assembling peptides form nanodiscs that stabilize membrane proteins.* Soft Matter, 2014. **10**(5): p. 738-52.

81. Oda, M.N., et al., *Cysteine substitutions in apolipoprotein A-I primary structure modulate paraoxonase activity.* Biochemistry, 2001. **40**(6): p. 1710-8.

82. Rosenblat, M., et al., *Paraoxonase 1 (PON1) enhances HDL-mediated macrophage cholesterol efflux via the ABCA1 transporter in association with increased HDL binding to the cells: a possible role for lysophosphatidylcholine.* Atherosclerosis, 2005. **179**(1): p. 69-77.

83. Watson, A.D., et al., *Protective effect of high density lipoprotein associated paraoxonase. Inhibition of the biological activity of minimally oxidized low density lipoprotein.* J Clin Invest, 1995. **96**(6): p. 2882-91.

84. Aviram, M., et al., *Paraoxonase active site required for protection against LDL oxidation involves its free sulfhydryl group and is different from that required for its arylesterase/paraoxonase activities - Selective action of human paraoxonase allozymes Q and R.* Arteriosclerosis Thrombosis and Vascular Biology, 1998. **18**(10): p. 1617-1624.

85. Mackness, M., P. Durrington, and B. Mackness, *Paraoxonase 1 activity, concentration and genotype in cardiovascular disease.* Curr Opin Lipidol, 2004. **15**(4): p. 399-404.

86. Harel, M., et al., *Structure and evolution of the serum paraoxonase family of detoxifying and anti-atherosclerotic enzymes.* Nat Struct Mol Biol, 2004. **11**(5): p. 412-9.

87. Sorenson, R.C., et al., *Human serum Paraoxonase/Arylesterase's retained hydrophobic N-terminal leader sequence associates with HDLs by binding phospholipids : apolipoprotein A-I stabilizes activity.* Arterioscler Thromb Vasc Biol, 1999. **19**(9): p. 2214-25.

88. Mishra, V.K., et al., *Lipid complex of apolipoprotein A-I mimetic peptide 4F is a novel platform for paraoxonase-1 binding and enhancing its activity and stability.* Biochem Biophys Res Commun, 2013. **430**(3): p. 975-80.

89. Gaidukov, L. and D.S. Tawfik, *High affinity, stability, and lactonase activity of serum paraoxonase PON1 anchored on HDL with ApoA-I.* Biochemistry, 2005. **44**(35): p. 11843-54.

90. Gaidukov, L., et al., *ApoE induces serum paraoxonase PON1 activity and stability similar to ApoA-I.* Biochemistry, 2010. **49**(3): p. 532-8.

91. Gugliucci, A., et al., *Enzymatic assessment of paraoxonase 1 activity on HDL subclasses: a practical zymogram method to assess HDL function.* Clin Chim Acta, 2013. **415**(16): p. 162-8.

92. Razavi, A., E., Ani, M., Pourfarzam, M., Naderi, G., A., *Associations between high density lipoprotein mean particle size and serum paraoxonase-1 activity.* Journal of Research in Medical Sciences, 2012. **17**(11): p. 1020-1026.

93. Gugliucci, A. and T. Menini, *Paraoxonase 1 and HDL maturation.* Clin Chim Acta, 2015. **439**: p. 5-13.